

İzmir Institute of Technology
Department of Mechanical Engineering

Design Project

ME402

Structural Improvement of a Wind Turbine Tower

Advisor: Assoc. Prof. Dr. Ünver Özkol

Cem Güngör	250203021
Mert Emrem	250203015
Sıla As	250203056

Spring 2021-2022

Contents

1	Introduction	1
1.1	Project Background	1
1.1.1	Brief History of Wind Energy	1
1.2	Aim of the Project	1
1.3	Design Criteria	2
2	Project Management	3
2.1	Project Timeline	3
2.2	Work Breakdown Structure	4
2.3	Linear Responsibility Chart	4
3	Literature Review	5
3.1	The Significance of the Structural Support	5
3.2	Connections of Structural Support	6
3.3	The Basics of the Dynamics of the Tower	6
3.3.1	1P Loading	6
3.3.2	3P Loading	8
3.3.3	Vortex Shedding	8
3.4	Optimization Approaches Used in Prior Studies	9
3.5	Additional Factors Regarding Structural Design	10
3.6	Application of Finite Element Method for Structural Analyses	11
4	Methodology	12
4.1	Design Studies	13
4.1.1	Design Parameters	13
4.1.2	Design Constraints	14
4.1.3	List of Assumptions	15
4.1.4	Design Loads	16
4.2	Analytical Modeling	23
4.2.1	Static Analytical Studies	24
4.3	Service Life & Fatigue Analyses	31
4.3.1	Developing an Analogous Model	31
4.3.2	Deriving Equivalent Ideal Elements	39
4.3.3	Damage Accumulation	44
4.4	Defining the Cost Function	45

4.5	Finite Element Analysis	48
4.5.1	Modal Analysis	50
4.6	Comparison of the Analytical and the FEA methods	51
5	Results and Discussion	52
5.1	Load Calculation	52
5.2	Optimization Results	56
5.3	Dynamic Study Results	59
5.4	Further Studies	62
5.4.1	Detailed Cost Analysis	62
5.4.2	Connections and the Foundation	63
5.4.3	Stiffeners	64
5.5	Finite Element Analysis	64
6	Conclusion	65
A	Appendix	69
A.1	Technical Drawings	69
A.1.1	Fastener Parts	69
A.2	MATLAB Code	69
A.2.1	Generating Graphical Results Given Set of Design Parameters . .	69
A.2.2	Optimization Study	78

List of Figures

1.1	The door detail of the reference model.	2
2.1	The Gantt chart of the project as conceived at the beginning of the project.	3
2.2	The revised and final Gantt chart of the project.	3
2.3	The linearized work breakdown structure of the project.	4
3.1	The number of yearly incidents caused by structural failures and blade-related failures between 2010 and 2020 [3].	5
3.2	L-type flanges by type: (a) slip-on flange, (b) welding-on flange, (c) welding-neck flange, (d) welding neck flange with defined contact area [5].	6
3.3	Model of the wind turbine showing reaction forces and moments, and centers of mass for rotor and nacelle as lumped point masses.	7
3.4	Von Kármán vortex shedding around a cylindrical body [8].	9
4.1	The overall methodology for the new design.	12
4.2	The illustration of the design parameters on the tower.	14
4.3	The illustration of the design parameters on the tower.	17
4.4	Strouhal - Reynolds Number relations for smooth and rough-surfaced bodies.	23
4.5	The relation between the analytical static and dynamic studies.	24
4.6	Flowchart of the optimization process.	25
4.7	Lumped-parameter system analogous to the tower.	32
4.8	Geometrical the relation between the horizontal deflection and true deflection.	33
4.9	Translational mechanical system representation of the lumped-parameter system.	34
4.10	Linear graph representation of the translational system shown in 4.9. . .	35
4.11	Diagram masses on the tower geometry including flanges.	37
4.12	Diagram of the translational mechanical system.	37
4.13	Diagram of the bending of one section within the Castigliano's second theorem calculation.	40
4.14	Spring element analogous of a shell section.	41
4.15	Probability density function of the wind speed, expressed as a Weibull distribution with $k = 2.47$ and $\lambda = 9.4$	45
4.16	The constituent parameters of the cost function.	46
4.17	Welding regions on the edges of shell elements [24]	47

4.18 The quasi-static analysis results of: (a) Reference tower at 36 m/s wind, (b) Reference tower at 52 m/s wind, (c) Proposed tower at 36 m/s wind, (d) Proposed tower at 36 m/s wind.	49
4.19 The 1 st and 2 nd eigenfrequencies (fore-aft, side-to-side respectively) of the reference (left) and the proposed (right) designs.	50
4.20 A partial model is obtained from a full model of the flange connection.	50
4.21 Left-to-right: A close-up view of the fastener mesh from the front, the side, and cross-section view.	51
 5.1 Force amplitudes acting on the RNA.	53
5.2 Force frequencies acting on the RNA.	54
5.3 Vortex shedding force amplitudes of the reference tower.	54
5.4 Vortex shedding force amplitudes of the proposed design.	55
5.5 Vortex shedding force amplitudes of the reference tower.	55
5.6 Vortex shedding force amplitudes of the proposed design.	56
5.7 The comparison of geometries of the reference (left) and proposed model (right).	58
5.8 The bode magnitude diagram of the reference tower.	60
5.9 The bode magnitude diagram of the proposed design.	60
5.10 The tip point deflection graph of the reference tower.	61
5.11 The tip point deflection graph of the proposed design.	61
5.12 The overall methodology for the new design.	64

List of Tables

2.1	Linear responsibility chart of the project	4
4.1	Design parameters chosen for analytical approach.	13
4.2	Design constraints chosen for analytical approach.	14
4.3	Material properties of S355JR, +AR [16].	15
4.4	Static and dynamic loads acting on the tower, as applied in the analytical method.	17
4.5	Calculated values for different ranges of height (z) [17].	21
4.6	Buckling coefficients for unstiffened cylindrical shells, mode a) Shell buckling.	28
4.7	Solver based nonlinear optimization methods in MATLAB [20].	30
4.8	Parts of the tower and their corresponding indices.	39
5.1	Calculated values for different values of height, z [9].	52
5.2	All of the calculated loads and moments for the wind speed of 36 m/s. .	52
5.3	All of the calculated loads and moments for the wind speed of 52 m/s. .	53
5.4	Parameters of the reference tower and the proposed design.	57
5.5	The cost comparison between the reference and proposed models.	58
5.6	Comparison of properties of the reference tower and the proposed design.	59

Abstract

Wind energy research has seen a significant increase as a result of the increasing energy demands of the world, and concerns of a global energy crisis. Onshore and offshore wind turbines are the most commonly used wind energy plants. In designing of a wind turbine, the factors of concern are efficiency, longevity, cost, and safety. The tower of the wind turbine is a critical component that affects all of these factors.

In this work, a specific 500 kW onshore tubular steel wind turbine tower has been provided as a reference design, with the aim of improvement by either: increasing the service life of the tower by 5%, or decreasing the cost of the tower by 5%, both without negatively affecting either parameter.

A methodology has been developed in order to obtain improved design using multi-objective optimization candidates and analytically assess and compare the said candidates with regards to the reference tower, in terms of buckling, static and dynamic behaviours, fatigue, and cost. The procedure included both analytical methods and FEM analyses to validate and further optimize the results.

The results that have been obtained by following this methodology satisfied the aforementioned criteria, and have been shown to be feasible. The proposed design yielded a 21.4% reduction in the cost of the tower, along with an increase in the service life of the tower.

Keywords: Wind Turbine, Tower, Fatigue, Analysis, Multi-objective optimization

Introduction

1.1 Project Background

The awareness around the looming global energy crisis has been the driving force of renewable energy research in the last decades. Wind energy comprises more than 6% of all energy produced globally as of 2021, with 743 GW in total, 707.4 GW of which is from onshore plants [1]. Wind turbines are currently the most commercially viable renewable energy source [2].

Though the energy generated by the movement of air has been harnessed by humanity for millennia, the rate at which the technology advances has increased rapidly in the last few decades to keep up with the increasing energy demand. Wind turbine producers are incentivized to design more cost effective towers in order to be competitive with not only fossil fuels, but also previous wind turbine designs.

1.1.1 Brief History of Wind Energy

As a result of the earth being heated unevenly by the sun, areas of high pressure and low pressure arise at different regions, which in turn causes convections in the atmosphere that we perceive as winds. Long have we harnessed the power of the winds, initially by setting sail out on the ocean, then by using it to grind grain, and since relatively recent times, to produce electricity.

The advent of wind turbines dates back merely around two centuries, with pioneers such as James Blyth and Charles F. Brush. Even the most primitive innovations in the field of electricity generation with wind turbines turned out to be exceptionally promising, as it required nothing more than a generator and a set of blades or sails, paired with a placement that sees a decent amount of wind. The wind turbines have been incrementally improved upon ever since, with the working principle remaining the same.

1.2 Aim of the Project

The project aims to improve upon an existing wind turbine tower design through the means of optimization. This was the approach that was decided to be suitable, as it results in a manageable scope, as opposed to other approaches of improving a wind turbine tower discussed in the later sections of this work. The overarching goal of the project is to contribute to the collective effort to make the switch to renewables by making

them more cost-effective.

1.3 Design Criteria

The primary design requirement of the project, as specified by the company, is either:

- A minimum of 5% increase in the service life of the tower with no increase in cost,
- A maximum of 5% decrease in the cost of the tower with no increase in service life.

The height of the tower is specified by the company to be 36 meters. See appendix for the technical drawing of the reference tower.

The material of the tower is specified as S355JR steel. The properties of this material are listed in section 4.1.2. Consideration of alternative materials is not within the scope of this project.

The reference tower has a door opening near ground level, and a collar stiffener around said opening, as shown by figure 1.1. Each fastening assembly connecting the flanges are comprised of the following:

- DIN931 - M 36 × 200 - 10.9 - KL steel hexagon head bolt
- DIN125 - A 37 - A4 steel washer
- DIN555 - M 36 - A3B steel nuts

The dimensions of the fasteners are included in the appendix. Further information with regards to technical details of each specification can be found through the corresponding standard for each item.

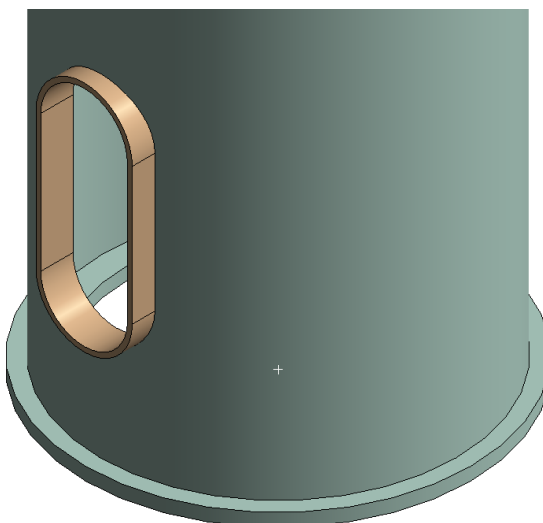


Figure 1.1: The door detail of the reference model.

Project Management

2.1 Project Timeline

The project spanned over two semesters. The Gantt chart created for the project has undergone minor changes: once to account for the delay in communication with the company, and once to adjust for the additional time added to the project. Our group was ahead of the schedule for the majority of the project. The initial and final Gantt charts are shown in figures 2.1 and 2.2 respectively. The tasks are further explained in the following sections.

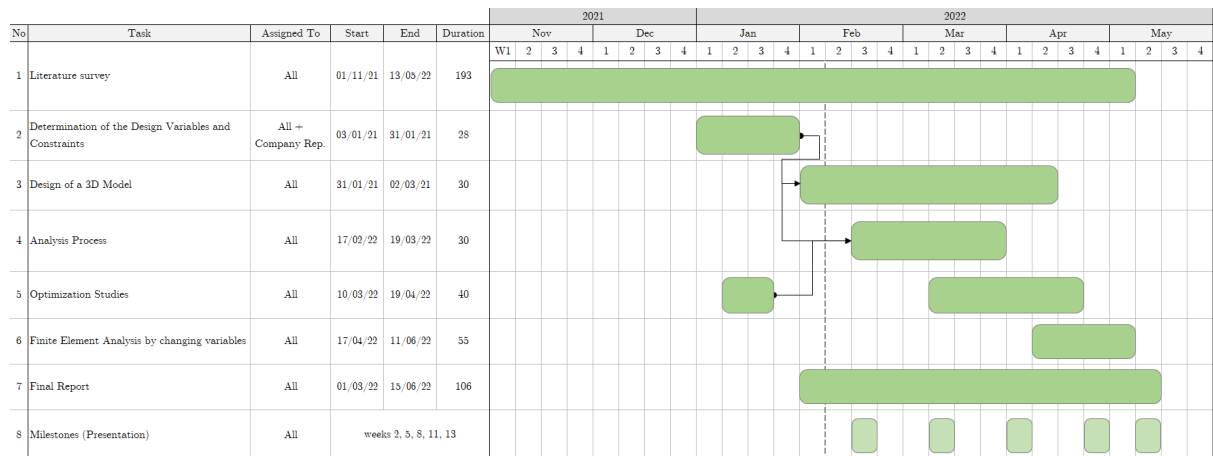


Figure 2.1: The Gantt chart of the project as conceived at the beginning of the project.

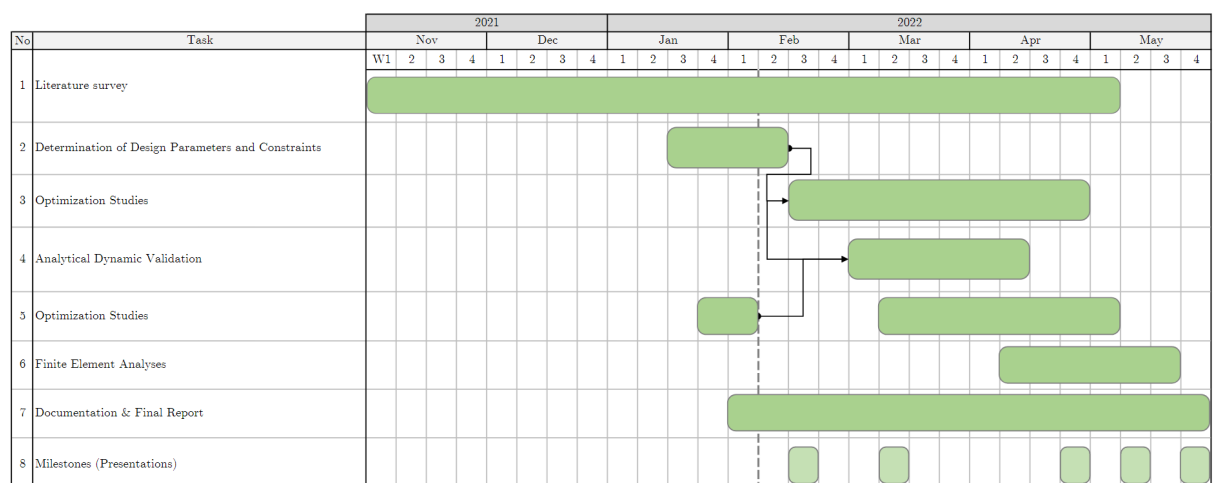


Figure 2.2: The revised and final Gantt chart of the project.

2.2 Work Breakdown Structure

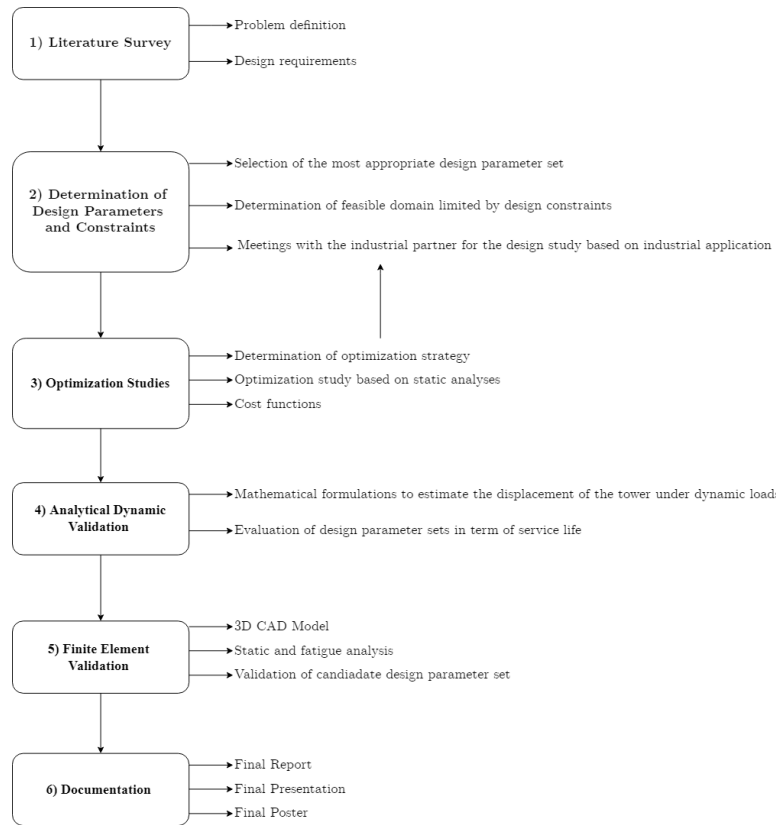


Figure 2.3: The linearized work breakdown structure of the project.

2.3 Linear Responsibility Chart

Table 2.1: Linear responsibility chart of the project

Task	Sıla As	Mert Emrem	Cem Güngör	Assoc. Prof. Ünver Özkol
Literature Survey	2	1	3	4
Determination of Design Parameters and Constraints	1	3	2	4
Optimization Studies	1	2	3	4
Analytical Dynamic Validation	3	2	1	4
Finite Element Validation	3	1	2	4

1: Primary	2: Secondary	3: Supportive	4: Advisor
------------	--------------	---------------	------------

Literature Review

3.1 The Significance of the Structural Support

According to one of the more comprehensive publicly available sets of data regarding wind turbine accidents and incidents, structural failures are the third most common cause of accidents, following blade failures and fire-related incidents [3]. As can be seen in figure 3.1, structural failures have consistently made up a large amount of WT failures.

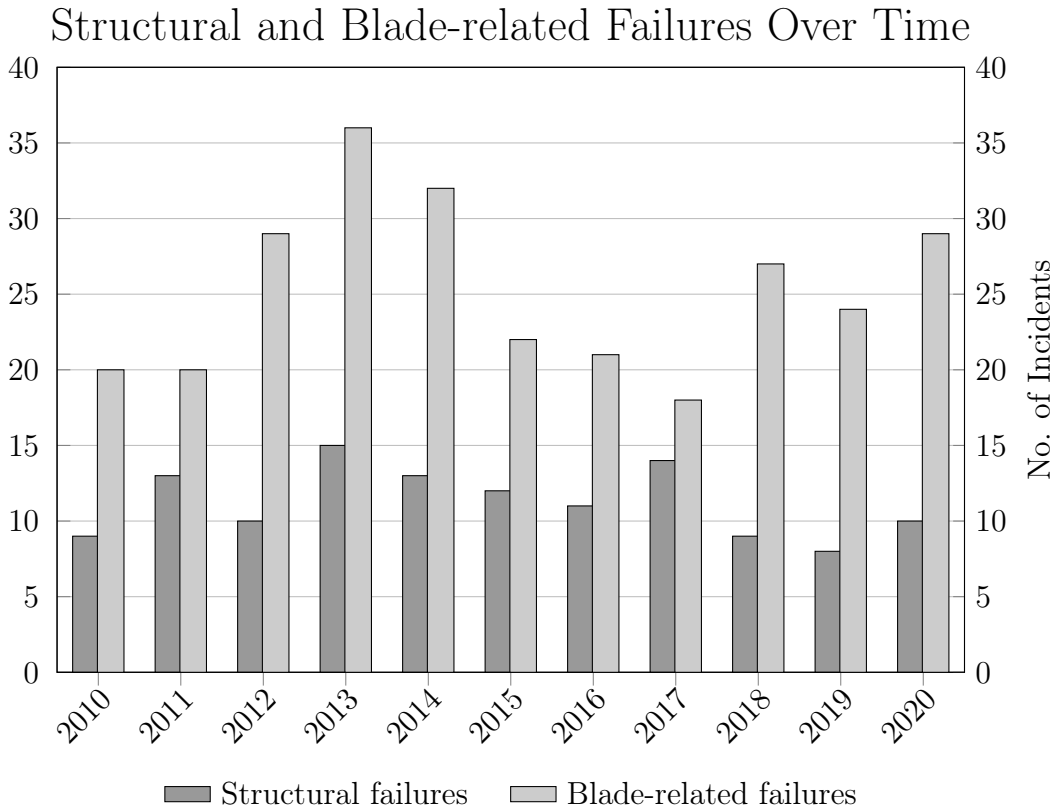


Figure 3.1: The number of yearly incidents caused by structural failures and blade-related failures between 2010 and 2020 [3].

In addition to its structural importance, the support also makes up around 16% of the installed cost for land-based WTs [4]. Another important consideration is that, if a turbine structure failure occurs, it is likely to lead to a total shutdown of the plant, even if the damage is partial. Many other parts of the plant can be recovered or replaced on failure after some downtime.

For small towers (1-500 kW), it is often the case that the effects of the dynamic

loads ignored, or accounted for by using safety factors, otherwise known as dynamic magnification factors. Since in this project, one of the ways in which the baseline tower can be improved is by making it more lightweight and therefore more vulnerable to resonances and structural instabilities, the same method cannot be applied, and the dynamic conditions must be examined.

3.2 Connections of Structural Support

The type of connection used in the reference tower provided are ring-flange connections, which are the most common type of joints in turbine towers of similar geometry to that of the reference tower [5]. This type of connection provides an easy assembling and disassembling process, as well as ease of replacement. Bolts involved in a ring-flange connection undergo high fatigue loading, and therefore are commonly investigated for fatigue behavior during the design process.

The shell elements are connected to each other using full-penetration butt welds. The connection between the shell elements and the flanges are also established through welding. The type used in the reference tower, as well as the type that is most commonly used in tubular turbine towers, is called an L-shaped ring-flange connection, named for its cross-sectional shape, as seen in figure 3.2. The specific type of connection of the reference tower is welding-on flange, as seen in figure figure 3.2 (b).

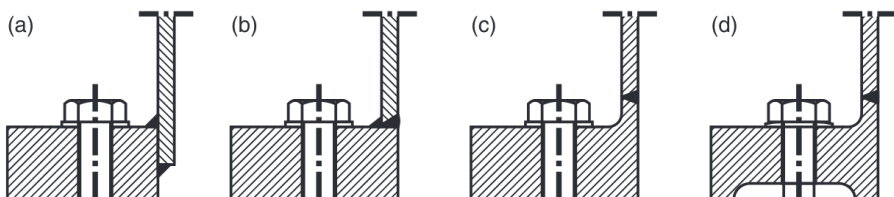


Figure 3.2: L-type flanges by type: (a) slip-on flange, (b) welding-on flange, (c) welding-neck flange, (d) welding neck flange with defined contact area [5].

Comparison of the types of flange connections are made in previous research [5], and is beyond the scope of this project.

3.3 The Basics of the Dynamics of the Tower

There are many dynamic loads in effect throughout the service life of a wind turbine, not all of which necessitate consideration. This section outlines the dynamic loads most commonly analysed in previous research.

3.3.1 1P Loading

The rotor of a WT introduces a cyclic loading to the system due to mass imbalance. If the wind turbine is pitch-controlled, an additional cyclic load due to aerodynamic im-

balance is induced [6]. For any given rotational speed of the wind turbine, 1P loading has constant frequency and amplitude, and is therefore modeled as F_c , with its dimensional components $F_{c,x}$, $F_{c,y}$, and $F_{c,z}$ as shown in figure 3.3 and equations 3.1. The amplitude A is determined by the mass and offset of this imbalance, m and R_m respectively, in addition to the rotational frequency of the rotor, ω . A is given a placeholder value based on the literature until it is provided by the company [7]. The frequency of this loading is defined by the rotational frequency of the tower, ω . The coordinate frame is defined at the base of the tower with x as the hub direction, and z as the axial direction of the tower.

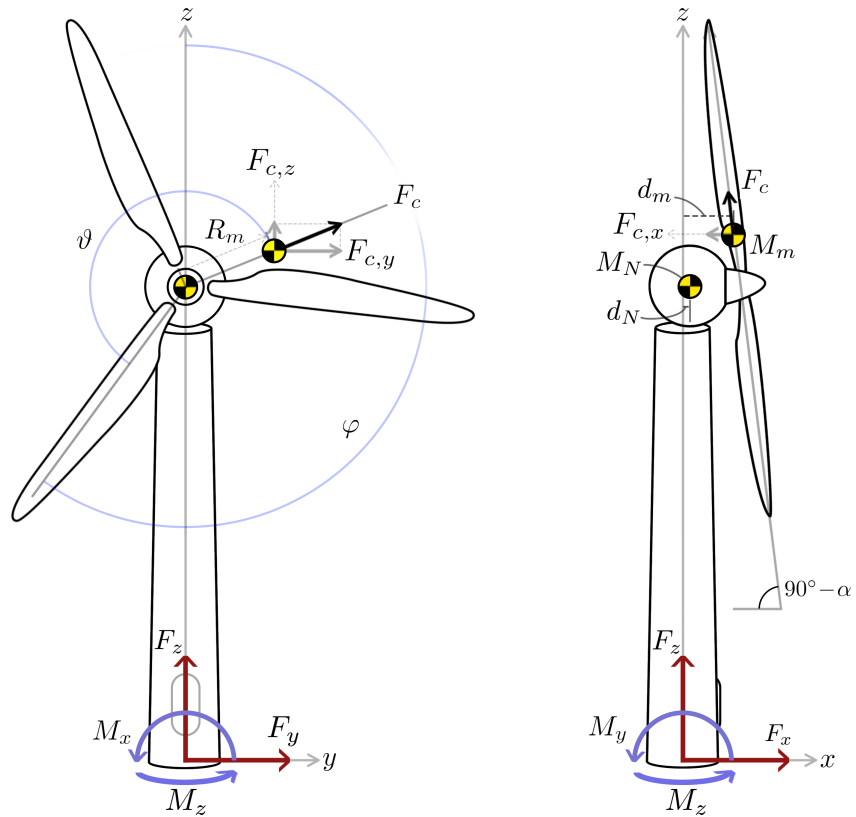


Figure 3.3: Model of the wind turbine showing reaction forces and moments, and centers of mass for rotor and nacelle as lumped point masses.

$$\begin{aligned}
F_c &= ma = mR_m\Omega^2 \\
F_c &= mR_m4\pi^2\omega^2 \\
F_{c,x} &= F_c \cdot \frac{\sin(\varphi + \vartheta)}{\cos \alpha} \\
F_{c,y} &= F_c \cdot \sin \alpha \\
F_{c,z} &= F_c \cdot \frac{\cos(\varphi + \vartheta)}{\cos \alpha}
\end{aligned} \tag{3.1}$$

The rotor of the WT may include a tilt angle, α . This is usually done as a measure against blade collisions with the tower under extreme loads. Since this parameter was not included in the specifications, α is assumed to be 0° to simplify the methodology, which can be modified to include it if needed. The angular offset, ϑ of the mass imbalance is also assumed to be 0° . These assumptions simplify the above equations to the following.

$$\begin{aligned}
F_{c,x} &= F_c \cdot \sin(\omega t) \\
F_{c,y} &= 0 \\
F_{c,z} &= F_c \cdot \cos(\omega t)
\end{aligned} \tag{3.2}$$

Meaning that in this case, no torsion is induced on the tower due to 1P loading. For small imbalance radii, the change in the height of $F_{c,y}$ will not cause significant changes in the reaction moments of the tower, and can therefore be neglected. Lever arm with regards to side-to-side motion is neglected as well. The justification for this assumption is that the centrifugal forces are more significant when compared to the moments created, and the model is simplified.

3.3.2 3P Loading

For a three-bladed WT, a blade passes headwind against the tower three times with each rotation of the rotor. This results in a disturbance in the flow and momentarily fluctuates the load on the tower. The frequency of this dynamic effect is three times that of the rotor frequency for a three-bladed wind turbine.

3.3.3 Vortex Shedding

When wind flows around a cylindrical object, a repeating pattern of swirling vortices form on the windward direction, arising in the wake of flows. The repeating pattern of swirling vortices are referred as the Von Kármán vortex street, shown in figure 3.4. The mechanism describing this phenomenon is known as the vortex shedding, where unsteady separation of flow around blunt bodies acts upon the body periodically. This phenomenon

causes lateral forces on the body around which it occurs.

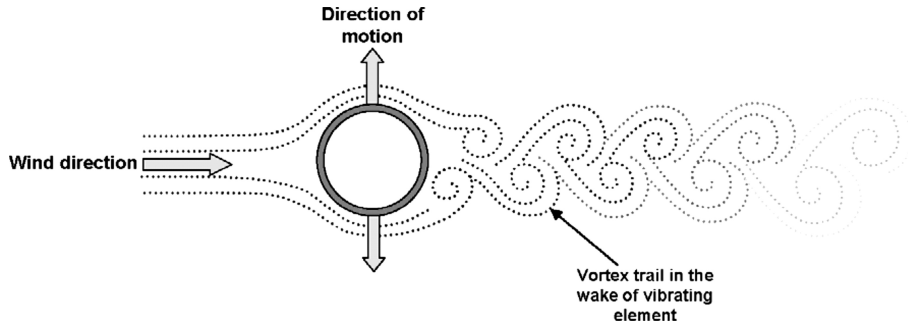


Figure 3.4: Von Kármán vortex shedding around a cylindrical body [8].

3.4 Optimization Approaches Used in Prior Studies

Structural design optimization of wind turbine towers have been studied intensively for a long time. These studies approach optimization of the tower from various perspectives. Depending on the tower property to be optimized, a different optimization strategy may have to be considered. Although their corresponding objective functions vary as well, the optimization is generally handled in three steps as follows [9].

- Defining the objective function
- Defining the design variables and boundary conditions
- Determining the design constraints

Though there are many properties of the tower that can be optimized, only several of them are commonly encountered in literature since they are able to offer relatively higher improvements in the tower design. The strategies involving these properties are listed below [9].

- Lightweight design

Minimizing the weight of the tower may lead to a significant reduction on the production cost and transportability of the tower. The method with which the weight is decreased is critical however, as it can decrease strength of the tower if the stiffness is reduced as a result of this optimization. This may lead to structural failure.

- High stiffness

High stiffness is critical in avoiding fatigue failure and provides structural stability since the higher stiffness corresponds to a reduced strains on the tower. It should be pointed out that the increase in the stiffness is mostly related to larger tower mass, which increases cost.

- High stiffness-to-mass ratio

Instead of considering the two criteria above individually, they can be combined to give better results in terms of both properties. This can be used to ensure that a proper trade-off between high stiffness and light weight is achieved.

- Design for minimum vibration

This strategy aims to minimize the motion of the tower so that the critical design targets, i.e. service life and stability are improved. There are two widely used methods in frequency domain, namely frequency-placement criterion and maximum frequency criterion. The frequency placement criterion utilizes an objective to move apart the natural frequencies of the tower from the excitation frequencies based on the forces acting on the tower. The maximum frequency criterion aims to maximize all natural frequencies of the tower regardless of the excitation frequencies. This way, the system response will be reduced when the tower is subjected to forces.

3.5 Additional Factors Regarding Structural Design

EN 1993-1-6 states that a hole in a shell may be neglected provided its largest dimension is smaller than $0.5\sqrt{rt}$, where r is the radius of shell where hole is located, and t is the thickness of the shell at said location [10]. In general, tower door openings do not meet this criterion, therefore this essential feature of the tower needs to be included in the analyses. The buckling of the door opening and buckling around the vicinity of the opening has been analysed by previous studies [11]. All such studies emphasize the reduced critical loads as a result of the door opening.

The fastening assemblies that are used to connect the flanges also necessitate more detailed analyses in order to ensure that the stresses that each one endures are below a certain limit. For fasteners, this limit is commonly proof strength rather than yield strength [12]. The aim of using the proof strength criteria is to prevent plastic deformation of the bolt, and is generally around 85-95% of yield strength. The fasteners are also subject to fatigue failure.

In wind turbine towers of similar configuration to the reference tower, cyclical loads on the fasteners are inevitable. To prevent the shortening of a bolt's fatigue life due to rapid load reversals, pre-tensioning is applied to each fastener at the assembly step. Pre-tension is the result of the stretching of a bolt due to over-tightening. Inadequate pre-tension may not meaningfully increase the fatigue life of a bolt, and excess pre-tension causes the bolt to plastically deform and accelerate cracking [12]. Unfortunately, there are no consistent, fail-proof methods of pre-tensioning threaded fasteners. Historically, it is often the case that over-designing such joints creates room for pre-tensioning inaccuracies, which may lead to severe failures. This is also a more economical approach compared to attempts at increasing assembling accuracy. The wide variety of real life complications

preclude any analytical formulations regarding this load. However, there exist methods of estimating pre-tension [12].

In order to distribute bearing stresses evenly, flange nuts or head bolts are used, alternatively, washers can be added to both the bolt head side and the nut side, in contact with the flanges. The literature shows the benefits of using of self-locking fasteners, such as wedge-lock washers [13]. Another important point is to ensure fasteners are protected from outside elements such as rain, as the lack of such protection may lead to premature fatigue [14].

3.6 Application of Finite Element Method for Structural Analyses

The finite element method (FEM) is a technique that enables the approximate solutions of boundary value problems [**shellthesis**]. At its modern state, FEM is employed almost exclusively by using computers. In FEM, the domain, such as the solid body to be analyzed, is discretized into many elements, each comprised of many nodes. The entirety of this discrete domain is referred to as the mesh model in finite element analysis (FEA) software. In building an FEA model, there are several factors to consider:

- Geometry: The FEA model needs to reflect the real-life body closely. Too much detail may lead to excessive computational loads however.
- Material: The material of each part should be described within the software, so that the results can be derived properly.
- Loads and boundary conditions: The physical effects such as gravity and external loads, along with conditions such as a stationary base should be represented reasonably.
- Part contacts: The ways with which the parts of the model interacts should be represented, such as frictional contacts.
- Mesh resolution: Dividing the model into more elements generally yields a more accurate result. However, increasing the element count also increases computation required to obtain a solution.

Methodology

This chapter outlines the overall methodology followed to achieve an improved design of the WTT. The methodology focuses on two study approaches: analytical studies and finite element studies. The main reason to proceed with the two parallel studies is that the most of the analysis parts can be conducted in analytical side by using comprehensive mathematical models. This way, achieving a new design parameter sets are much faster compared to time consuming optimization process in Finite Element Analysis. The analytical model has many assumptions that make the analytical model less realistic. Therefore, the outcomes of the analytical studies (the design parameter set) is to be validated in the FEA part. In case the FEA studies show an infeasible solution with these design parameters, the analytical model is updated based on the insight obtained from FEA. Additionally, analytical studies are divided into static and dynamic studies. The flow chart in figure 4.1 demonstrates the overall design strategy in the project based on an iterative approach and the relationships between each study which are explained in detail in the further sections.

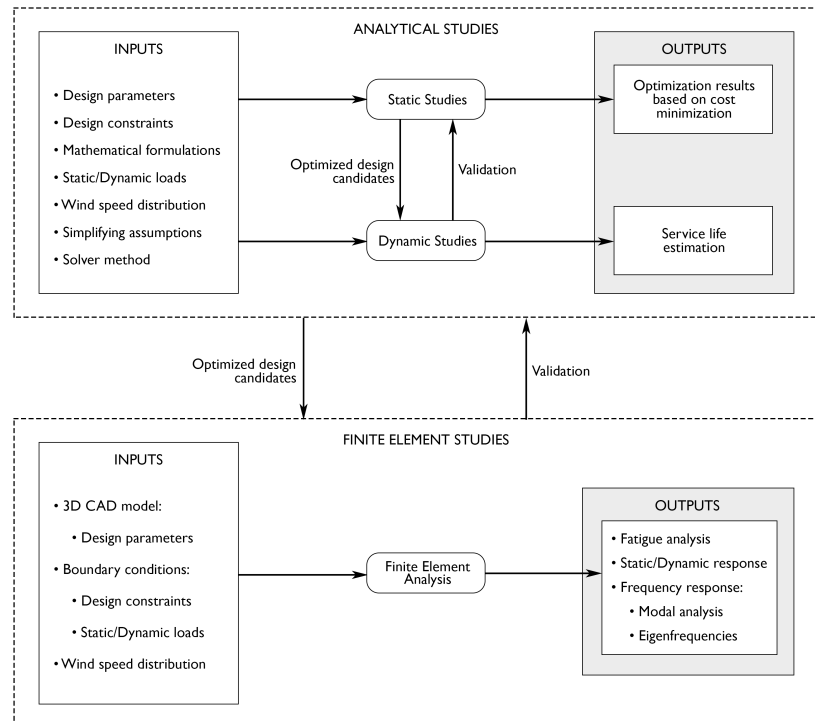


Figure 4.1: The overall methodology for the new design.

4.1 Design Studies

As explained in the previous passage, the studies in this project have been conducted either analytically and numerically, via finite element method. Although these two approaches use different methods, and are based on different assumptions, the properties of interest of the system to be optimized, in this case the WTT, must be identical. This corroborates that the outcomes of the both studies are comparable and usable for the iterative approach. The considered baseline properties can be listed under 3 titles, which are design parameters, design constraints and assumptions.

4.1.1 Design Parameters

Design parameters stand for changes in the system model, in this case they are parameters of the tower, to achieve desired improvement goals.

As defined in section 1.3, the project aims to achieve either of the following goals:

- Maximized service life of the tower
- Minimized cost of the tower

By considering the goals above, the design parameters were determined carefully such that the same set of design parameters can be used for either approach. This reduces modelling and analysis effort significantly.

Literature review reveals that cost minimization is highly related to decrease in mass for the wind turbine towers. Therefore, upon investigating the ways of minimization of the mass, it is concluded that the geometrical parameters of the tower greatly affect the tower mass [9]. Although there are many ways to manipulate the geometrical properties, several of them were chosen as design parameters, after all the possible design parameters were evaluated by considering the ease of modeling and analysis, given the limited project resources. The determined design parameters are illustrated in figure 4.2 and listed in table 4.1.

Design Parameters	
Height of a section	H_1, H_2, H_3
Thickness of shell at a section	t_1, t_2, t_3
Base diameter	D_1
Growth rate of a section	g_1, g_2, g_3

Table 4.1: Design parameters chosen for analytical approach.

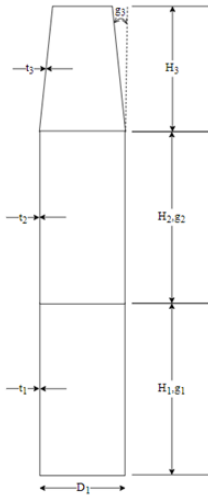


Figure 4.2: The illustration of the design parameters on the tower.

In addition, the geometrical properties considerably affect the stiffness of the tower, which is directly linked to the service life of the tower. Maximization of the service life is obtained by optimizing the stiffness of the tower. Through this method, it can be guaranteed that the design parameters have a serious impact on either the minimization of the cost or maximization of the service life.

Design Constraints

- Buckling failure limit
 - Dynamic fatigue failure limits < and excitation frequencies
 - Manufacturing limitations
 - Tapering limitation
 - Transportation limitation
 - Stiffness and damping coefficient limitations from mass minimization
 - Additional specifications provided by industrial partner
-

Table 4.2: Design constraints chosen for analytical approach.

4.1.2 Design Constraints

Design constraints describe the limitations of the design parameters based on possible failures and undesirable situations, and they can be expressed mathematically. Design constraints are very important to determine the feasible domain of the design parameters. There are many undesirable situations that can arise , and the design must regard these undesirable situations in order to avoid them. In this way, the most significant of the predictable failures can be alleviated. In our case, the design constraints are due to the following reasons, in no particular order [15].

- Static failures due to buckling stresses
- Dynamic failures due to fatigue and exciting the tower natural frequency
- Manufacturing limitations
- Tapering limitations
- Transportation limitations
- Stiffness and damping coefficient limitations derived from mass minimization
- Specifications determined by the company

The details of the design parameters are explained in section 4.2.

Failure criteria are governed by the material properties, such as yield strength, maximum allowable shear etc. The material used for the tower is S355JR, +AR, properties of which are shown in table 4.3.

Property	Symbol	Thickness	Value	Unit
Density	ρ		7800	kg/m ³
Young's modulus	E		210	GPa
Shear modulus	G		80	GPa
Poisson's ratio	ν		0.30	-
		≤ 16 mm	355	
Tensile yield strength	σ_y	16-40 mm	345	MPa
		40-63 mm	335	

Table 4.3: Material properties of S355JR, +AR [16].

4.1.3 List of Assumptions

Assumptions are essential parts in simplifying a study in an efficient and realizable way. In the real world, there are thousands of factors affecting the system, but only a select few are dominant, in that they manipulate the behavior of the system more than others. Therefore, the less significant external effects can be neglected, with the help of a comprehensive literature review and engineering insight. In our case, the wind turbine is exposed to many various forces, moments, wind velocities, extreme cases such as earthquakes etc. Only the set of the external effects which are listed below are taken account. As two distinct approaches were applied, two sets of assumptions were used to model the problem.

The assumptions made for the analytical studies are as follows.

1. In static studies, shear and torsion forces are neglected due to their relatively insignificant effect on the bending moment of the tower.
2. Each section is treated as a single part with uniform cross-section varying only in diameter. as opposed to taking into consideration the butt-jointed shell subsections.
3. Friction at flange contact, bolt connections and holes, and bolt pretension are neglected.
4. Two major velocities are considered: rotor braking wind speed of 36 m/s, and 52 m/s, which is the specified extreme condition by IEC 61400.

The assumptions made for the FEA studies are as follows.

1. The tower is cantilevered to the ground. The ground connection surface is constrained in all directions and rotations.
2. The effect of bolt pre-tension can be neglected for the full model.
3. Friction between flanges, and the friction between the bolt heads and the flanges are defined.
4. Harmonic Analysis:
 - All dynamic loads are sinusoidal and have the same frequency.
 - Transient effects are negligible, and steady-state of the structure is solved.

4.1.4 Design Loads

In reality, a wind turbine is exposed a complex set of loads. However, in the project, only the most significant ones are considered to reduce the complexity and time consumption on the load calculation. The loads acting on the tower can be expressed as two types of loads which are static and dynamic loads. All these forces are listed in table 4.4 with their descriptions, and are illustrated in figure 4.3.

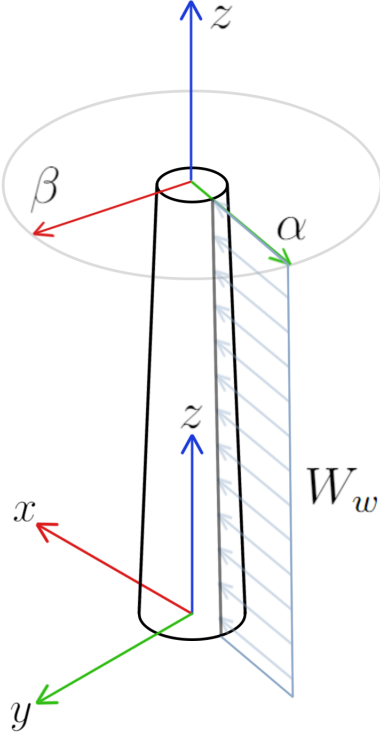


Figure 4.3: The illustration of the design parameters on the tower.

	Load Type	Description	Dir.	Symbol	Applied Region
Static	Point	Assembly Weight	$-z$	F_{RNA}	Tip point
	Point	Rotor thrust force	$-\alpha$	F_T	Tip point
	Distributed	Tower Weight	$-z$	W_t	Throughout tower
	Distributed	Wind load on tower	$-\alpha$	W_w	Throughout tower
	Moment	Due to RNA CoM offset	$-\beta$	M_{RNA}	Tip point
Dynamic	Point	Centrifugal force of rotor	β	F_r	Tip point
	Point	Force due to blade passing	β	F_b	Tip point
	Point	Vortex shedding force	β	F_v	Throughout tower

Table 4.4: Static and dynamic loads acting on the tower, as applied in the analytical method.

Static Loads

The tower is subjected to the wind loads which result in thrust force by the rotor and aerodynamic loads on the tower directly. Additionally, the weight of the RNA creates a significant axial load on the tower, as well as significant moment due to eccentricity of the center of mass of rotor nacelle assembly. Finally, the moment that originates from

the thrust force acting on the rotor is also significant.

Before the calculation of these terms, several conditions must be defined. The reference speed is a determining factor for the calculations of the loads. For both analytical and FEA studies, all the design variables must be checked in terms of static analysis at where the loads and moments create maximum impact. Following these steps confirms that the proposed design is able to withstand the extreme loads which occur at maximum speed of wind before the rotor stops rotating. Based on the cut-out speed (25 m/s) that is given for the reference model, the reference velocity which is used in further aerodynamics loads calculations is determined as 36 m/s [17].

- Load in axial direction due to tower mass (W_t)

The weight of the tower is calculated based on the equation 4.1. The specific properties of the material used can be found in table 4.3.

$$W_t = \rho V g \quad (4.1)$$

Where ρ , is the density of the material, V is the volume of the tower and g is gravitational acceleration.

- Load in axial direction due to rotor nacelle assembly (F_{RNA})

The information of the rotor nacelle mass is provided by our industrial partner. The weight rotor nacelle assembly is constant throughout all studies.

- Moment due to eccentricity of the assembly (M_{RNA})

Based on the technical drawings provided by our industrial partner, the moment due to eccentricity of the assembly weight with respect to the vertical axis of the tower can be calculated.

- Thrust force due to wind (F_T)

The thrust force acting on the rotor due to aerodynamic load is calculated using equation 4.2.

$$F_T = \frac{1}{2} C_T A V_{ref}^2 \quad (4.2)$$

Where C_T is thrust coefficient, determined as 0.1583 for the reference wind velocity of 36 m/s [17], A is the swept area of the rotor, which is πR^2 , R being the rotor radius,

v_{ref} is the reference velocity.

Although the dimensional and geometrical information about the tower is provided, any specific dimensional information about the rotor was not provided. Therefore, the diameter of the rotor was not specified. However, detailed information about 350 kW wind turbine was provided. By using the information of 350 kW wind turbine, a similitude study is executed to estimate a reasonable radius for the rotor of the 500 kW wind turbine.

Similitude Study

By applying the Buckingham Pi Theorem, it is observed that power coefficient is a function of the Reynolds and Mach Numbers. It can be assumed that Reynolds number for both of sizes are approximately similar and can be neglected for high values. Also, the Mach Number can be assumed as less than 0.3 for both of them, therefore it is taken as non-effective independent variable as well. Therefore, it can be concluded that both turbines have similar power coefficients.

The power coefficient C_p is defined in equations 4.3 and 4.4.

$$C_P = (\text{Re}, \text{Mach}) \quad (4.3)$$

$$C_P = \frac{P}{\frac{1}{2} \rho A V_{\text{ref}}^3} \quad (4.4)$$

Where P is the power of the wind turbine, A is the rotor swept area. The similitude rule is expressed as equation 4.5.

$$(C_P)_{350 \text{ kW}} = (C_P)_{500 \text{ kW}} \quad (4.5)$$

Additionally, the reference velocities are defined as 14 m/s for the 350 kW turbine and 15 m/s for the 500 kW turbine. These velocities are the specified rated wind velocities (i.e. operational speed). Also, the rotor radius for the 350 kw turbine is 17.643 m.

$$\frac{350 \text{ kW}}{\frac{1}{2} \left(1.2 \frac{\text{kg}}{\text{m}^3} \right) \pi (17.643 \text{ m})^2 \left(14 \frac{\text{m}}{\text{s}} \right)^3} = \frac{500 \text{ kW}}{\frac{1}{2} \left(1.2 \frac{\text{kg}}{\text{m}^3} \right) \pi (R_{500kw})^2 \left(15 \frac{\text{m}}{\text{s}} \right)^3} \quad (4.6)$$

Using equation 4.6, the $R_{500\text{kW}}$ is found to be 19.014 m. Through these calculations, thrust force is obtained.

- Moment due to the thrust force (M_T)

The moment due to the thrust force with respect to the tower tip can be calculated for a given hub height.

- Load on the tower due to wind (W_w)

Based on Eurocode [18], the average wind load on the tower is calculated using equation 4.7.

$$W_w = q_{\text{ref}} c_e(z) c_d c_f D \quad (4.7)$$

Where $q_{\text{ref}} = \frac{\rho}{2} V_{\text{ref}}^2$, D is the effective diameter, c_f is the force factor, c_d is the drag coefficient, and $c_e(z)$ is the related factor expressed in further steps [17].

Factor $c_e(z)$ is calculated using equation 4.8.

$$c_e(z) = c_r^2 c_t^2 (1 + 2g l_v) \quad (4.8)$$

Where $g = 3.5$, z is the height in meters, $l_v = \frac{k_r}{c_r c_t}$ where $k_r = 0.17$, $c_t = 1$.

Finally, c_r is calculated using equation 4.9.

$$c_r = k_T \ln \left(\frac{z}{z_0} \right) \quad (4.9)$$

All the values are assigned as proposed by Farkas et al. [17], whose work has references similar studies. Therefore, it is assumed that the wind loads on the tower for the reference wind turbine are defined with similar coefficients. These values are listed in table 4.5.

z (m)	c_r	l_v	c_e
24-36	1.43	0.119	3.747
12-24	1.36	0.125	3.468
0-12	1.24	0.137	3.012

Table 4.5: Calculated values for different ranges of height (z) [17].

In addition, drag coefficient c_d and c_f are determined as 1.1 and 0.825 respectively [17].

Dynamic Loads

Four main sources of dynamic force that have prominent effect on the fatigue life of the tower structure are identified as following:

Description	Notation	Applied region	Model
Force due to rotor mass imbalance	F_r	Assembly	Ideal force source
Aerodynamic response of the blade passing in front of the tower	F_b		
Cyclical loading due to vortex shedding	$F_{v,i}$	Tower	
External forces due to tectonic activities	F_t	Ground	Ideal velocity source

The effects of tectonic activities on the tower is excluded to limit the scope of the project to loads due to effect of the wind. The dynamic forces in this case can be classified based on which section of the tower that the load is acting on.

Dynamic Forces acting on the Rotor-Nacelle Assembly As discussed prior, rotor and blade forces acts cyclical whose magnitudes with respect to the wind speed can be described as shown in equation 3.1. The dynamic load due to rotor and blade forces acting as a point load can be expressed as

$$|F_r| \sin(\omega_r t + \varphi_r) + |F_b| \sin(\omega_b t + \varphi_b) \quad (4.10)$$

The frequency associated with the rotor and blade forces is expressed as

$$\omega_r = \frac{\pi U_r}{30} \quad (4.11)$$

(4.12)

$$\omega_b = \frac{\pi U_r}{10} \quad (4.13)$$

Where U_r is the rotor speed.

Since the power output of the turbine is linear to the rotor speed, a relation between the power curve of the wind turbine and the rotor speed can be made. Given wind turbine specifications for the reference model, the rotor speed – wind speed relation is shown as

$$U_r(v) = \begin{cases} 0 & \text{if } v < 4 \text{ and } v > 25 \\ \frac{25v - 100}{11} & \text{if } v \geq 4 \text{ and } v < 15 \\ 25 & \text{if } v \geq 15 \text{ and } v \leq 25 \end{cases} \quad (4.14)$$

Dynamic Forces Acting on the Tower The most prominent effect of the vortex shedding is that the body experiences significant vibration perpendicular to the wind direction, therefore the forces associated with the vortex shedding (explained in section 3.3.3), can be modeled as a sinusoidal load.

A vortex street only forms when a certain threshold of flow velocity is achieved. This threshold varies by the shape and the surface roughness of the body. The relation between the vortex shedding frequency is calculated by

$$\omega_v = \frac{2\pi St}{D} \quad (4.15)$$

Where St is Strouhal number and D is the outer diameter of the body. Strouhal number is a dimensionless number derived empirically, describing the relation between the Reynolds number and the vortex shedding frequency. This relation is shown in figure 4.4.

Strouhal number is a dimensionless number derived empirically, describing the relation between the Reynolds number and the vortex shedding frequency. The relation is

shown in fig. x. for smooth and rough cylinders.

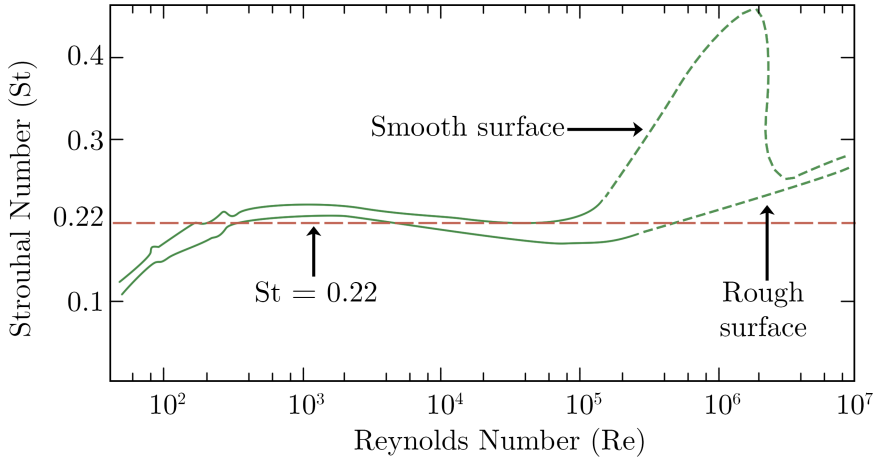


Figure 4.4: Strouhal - Reynolds Number relations for smooth and rough-surfaced bodies.

In this study, Strouhal number is assumed to be constant and equal to 0.22 since the surface roughness of the tower is not known. For the magnitude of the vortex shedding force, a dynamic force factor of 0.25 is provided from the literature. This expresses the ratio between the static thrust force of the wind and the amplitude of the dynamic forced that is applied. Therefore:

$$F_v = |F_v| \sin(\omega_v t) = \frac{F_t \sin(\omega_v t)}{4} \quad (4.16)$$

4.2 Analytical Modeling

As mentioned in the beginning of the chapter, the analytical model enables rapid progression since most of the properties of the tower can be described analytically, based on a set of assumptions. However, it should be pointed out that the outcomes of the analytical studies do not cover all the aspects of the complex engineering design. Therefore, the outcomes must be validated by FEM analyses.

The analytical studies are carried out in two sections, which are static and dynamic studies. The static studies are based on six major external and gravitational forces and moments. In this study, the possible failures and limitations such as buckling, excitatory frequencies of the tower with regards to changes in stiffness and damping ratio, transportation and manufacturing limitations are considered as constraints, and a feasible domain which limits appropriate sets design parameters is obtained. The static studies

are considered an optimization problem, and mainly focus on the cost minimization since the cost of the tower is directly related to the mass of the tower, and the process of formulating the objection function of the mass is straightforward.

On the other hand, the dynamic studies are critical in assessing eventual failure that may be caused by fatigue loads. In this study, oscillation of the tower within a specific time interval is linked to the service life of tower in MATLAB/Simulink. In the dynamic studies, the design parameter set that is optimized in the static studies is used as an input. This way, the optimized design parameters based on the mass minimization are validated in terms of fatigue behavior. The relationship between the analytical static and dynamic studies is described in figure 4.5.

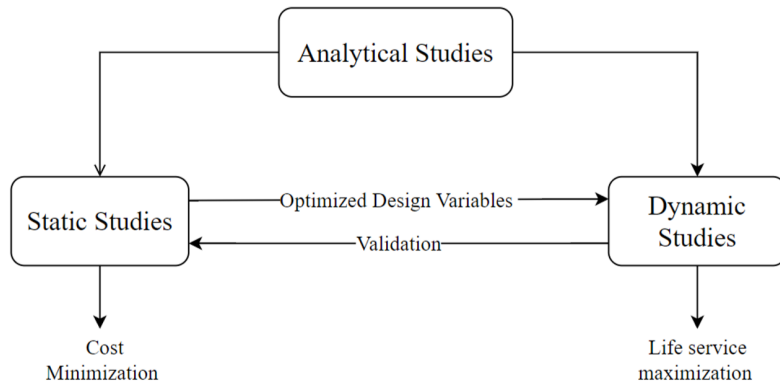


Figure 4.5: The relation between the analytical static and dynamic studies.

4.2.1 Static Analytical Studies

The optimization part of the project is covered in the analytical static studies. In other words, the feasible domain obtained from static analysis is used to acquire optimized values of the design variables based on what it is needed to maximize/minimize. Therefore, the entire study is treated as an optimization problem. Generally, the optimization problems are described in four steps, as shown in figure 4.6.

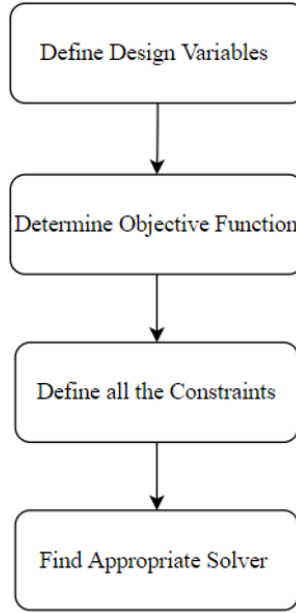


Figure 4.6: Flowchart of the optimization process.

In the project, two properties of the tower, the mass and the stiffness are studied to minimize and maximize respectively within the static studies. However, only the cost minimization is taken as a baseline since its objective function gives more realistic outcomes and a faster solution, considering the limited project period. However, in the case that results of minimization of mass cannot be validated in FEA, the stiffness maximization will be considered instead.

Defining the Design Parameters

The set of design parameters have been determined as shown in table 4.1 in section 4.1.1.

Defining the Objective Function

Based on goals of the project, two optimization strategies have been chosen: mass minimization and stiffness maximization of the tower. However, in this project the mass minimization is the main consideration. Its objective function considers either mass of the tower, M , which can be calculated by multiplying the density, ρ , and the total volume, V_{total} of the material. This objective function is defined as equation 4.17.

$$M = \rho V_{\text{total}} \quad (4.17)$$

Where V_{total} can be expressed as

$$V_{\text{total}} = \sum_{i=1}^n V_i \quad (4.18)$$

Where V_i is the volume of the i^{th} component of the tower and is calculated as follows. In our case, the tower is divided into a total of 9 components: 3 shells and 6 flanges. Note that the design parameters determined in section 4.1.1 only apply to the shell elements.

$$V_i = \pi t_i h_i (D_i - g_i H_i) \sqrt{g_i^2 + 1} \quad (4.19)$$

Defining the Constraints

- **Tapering Limitation:** The diameter of the tower must decrease as the height increases [15].

$$D_{i+1} \leq D_i \quad (4.20)$$

- **Manufacturing Limitation:** A limit is assigned for the aspect ratio between the thickness and diameter of the shell [15].

$$t_i - 0.008D_i \leq 0 \quad (4.21)$$

- **Transportation Limitation:** The diameter of the tower must be less than 4.5 m to allow for roadway transport under highway bridges and through tunnels [15].

$$D_i \leq 4.5 \text{ m} \quad (4.22)$$

- **Damping Coefficient Constraint:** Damping coefficient determines the magnitudes of natural frequency excitations of the tower and as it decreases, the tower excites more severely. Therefore, the ratio must be constant to keep the service life of the tower constant when the mass is minimized. The relation of the damping ratio is shown in equation 4.23.

$$b_{\text{initial}} \cong b_{\text{optimized}} \quad (4.23)$$

Where b_{initial} is the damping coefficient of the reference model and $b_{\text{optimized}}$ is the damping coefficient of the optimized design. The damping ratio is calculated using equation 4.24.

$$b = 2\zeta\sqrt{MS_{\text{overall}}} \quad (4.24)$$

Where ζ is the damping ratio and S_{overall} is the overall stiffness of the tower.

- **Buckling Stress Constraint:** The buckling constraint is a very significant constraint that designers should consider in the optimization process. The tower must not buckle due to external loads and moments. Therefore, the sum of the axial stresses, σ_a , and bending stresses, σ_b , must be less than the critical buckling stress, σ_{cr} [17].

$$\sigma_{\text{max}} > \sigma_a + \sigma_b \quad (4.25)$$

$$\sigma_a = \frac{G_w}{D\pi t} \quad (4.26)$$

$$\sigma_b = \frac{4\gamma M_w}{\pi D^2 t} \quad (4.27)$$

Where

G_w : Axial load on the shell segment

M_w : Moment on the shell segment

γ : Safety factor for the effective moment [10].

$$\sigma_{cr} = \frac{F_y}{\sqrt{1 + \lambda^4}} \quad (4.28)$$

Where

f_y : Yield stress

λ : Reduced slenderness

$$\lambda^2 = \frac{f_y}{\sigma_a + \sigma_b} \left(\frac{\sigma_a}{\sigma_{Ea}} + \frac{\sigma_b}{\sigma_{Eb}} \right) \quad (4.29)$$

Where

σ_{Ea} : Axial elastic buckling stress

σ_{Eb} : Reduced Bending elastic buckling stress, which are defined as follows.

$$\sigma_{Ea} = (1.5 - 50\beta) C_a \frac{\pi^2 E}{12(1 - \nu^2)} \left(\frac{t}{H} \right)^2 \quad (4.30)$$

$$\sigma_{Eb} = (1.5 - 50\beta) C_b \frac{\pi^2 E}{12(1 - \nu^2)} \left(\frac{t}{H} \right)^2 \quad (4.31)$$

Where

ν : Poisson's ratio of the material

β : Reduction factor caused by radial deformation factor due to the shrinkage of circumferential weld. It is assumed 0.02 [17].

C_a : Reduced axial buckling coefficient

C_b : Reduced bending buckling coefficient, which are defined as follows.

$$C_a = \sqrt{1 + (\rho_a \xi)^2} \quad (4.32)$$

$$C_b = \sqrt{1 + (\rho_b \xi)^2} \quad (4.33)$$

The parameters to calculate C_a and C_b are taken from table 4.6 from DNV [19].

Coefficient	ξ	ζ	ρ
Axial stress	1	$0.702Z$	$\frac{0.5}{\sqrt{(1 + \frac{r}{150t})}}$
Bending	1	$0.702Z$	$\frac{0.5}{\sqrt{(1 + \frac{r}{300t})}}$
Torsion and shear force	5.34	$0.856Z^{3/4}$	0.6
Lateral pressure	4	$1.04\sqrt{Z}$	0.6
Hydro-static pressure	2	$1.04\sqrt{Z}$	0.6

Table 4.6: Buckling coefficients for unstiffened cylindrical shells, mode a) Shell buckling.

$$\rho_a = \frac{0.5}{\sqrt{(1 + \frac{r}{150t})}} \quad (4.34)$$

$$\rho_b = \frac{0.5}{\sqrt{(1 + \frac{r}{300t})}} \quad (4.35)$$

$$\zeta = 0.072Z \quad (4.36)$$

$$Z = \frac{L^2}{Rt} \sqrt{(1 - \nu^2)} \quad (4.37)$$

- **Stiffness Constraint:** It is essential to keep the stiffness of the tower at a reasonable value as the mass of the tower decreases. Therefore, it is decided to limit the allowable stiffness reduction to 5%.

$$S_{\text{reference}} - 1.05S_{\text{optimized}} \geq 0 \quad (4.38)$$

Where

$S_{\text{reference}}$: Stiffness of the reference tower

$S_{\text{optimized}}$: Stiffness of the optimized tower

$$S_i = \frac{Et_i\pi\sqrt{g_i^2 + 1}}{8 \int_0^H (H_i - z)^2 (D_i - 2g_i z) (4g_i^2 z^2 + g_i^2 t_i^2 - 4D_i g_i z + t_i^2 + D_i^2) dz} \quad (4.39)$$

The S_i refers to each section's stiffness. The total stiffness, S_{total} , is calculated as

$$S_{\text{total}} = \sum_{i=1}^3 S_i^{-1} \quad (4.40)$$

- **Company Specifications:** The only constraint stipulated by the company is that the total height of the tower must be fixed at 36.5 m.

$$H_1 + H_2 + H_3 = 36.5 \text{m} \quad (4.41)$$

Choosing an Appropriate Solver

There are a variety of solvers that can be used to optimize a property (in this case, the mass of the tower). Depending on the objective function and constraints, only a few of them are capable of handling the optimization problem. The constraints which are given in section 4.2.1 are defined by nonlinear functions, equations and inequations with certain lower and upper bounds. Solver based nonlinear optimization methods within Matlab Optimization Toolbox are given in table 4.7.

Solver-Based Nonlinear Optimization Functions

<code>fminbnd</code>	Minimum of single-variable function on fixed interval
<code>fmincon</code>	Minimum of constrained nonlinear multivariable function
<code>fminsearch</code>	Minimum of unconstrained multivar. function using derivative-free method
<code>fminunc</code>	Minimum of unconstrained multivariable function
<code>fseminf</code>	Minimum of semi-infinitely constrained multivariable nonlinear function

Table 4.7: Solver based nonlinear optimization methods in MATLAB [20].

From the table above, the only appropriate solver function which meets the requirements is the `fmincon` function [21].

The function `fmincon` requires several inputs to be executed. These inputs are as follows.

$$[x] = \text{fmincon}(\text{fun}, x_0, A, b, A_{\text{eq}}, b_{\text{eq}}, l_{\text{eq}}, u_{\text{eq}}, \text{nonlcon}) \quad (4.42)$$

- $[x]$ is the set of optimized design parameters
- `fun` is the objective function of mass of the tower
- x_0 is the initial value where the search of the feasible domain is initiated, in this case the initial value is the reference model's own values
- A describes the coefficient matrix of the design variables and b is the corresponding value to define the inequality constraints as $Ax \leq b$
 - Manufacturing limitations
 - Aesthetic limitations
- A_{eq} describes the coefficient matrix of the design variables and b_{eq} is the corresponding value to define the equality constraints as $A_{\text{eq}}x = b_{\text{eq}}$
 - The total height of the tower is fixed

- A_{eq} and A_{eq} correspond to lower and upper bounds of the design variables respectively.
- **nonlcon** is the set of other constraints.

The **fmincon** algorithm aims to find local minimum values in the feasible domain that is restricted by the constraints. Iteratively, it evaluates the objective function by modifying design parameters until the gradient of the objective function is approaching zero, at which point the function locates the local minima.

4.3 Service Life & Fatigue Analyses

The aim of the service life and fatigue analysis study is to provide insight regarding how a given design parameter set performs in terms of service life. Carrying out fatigue analysis for a finite element model is computationally expensive, therefore, developing quantitative means to assess the feasibility of a given parameter set beforehand serves a crucial purpose.

In the service life and fatigue analysis study, only the forces associated with the effects of wind are considered, however, the model of the study can be advanced further by following the methodologies and principles that are presented in this section.

Representing the tower as a mathematical model is done under two subsections. These include: (1) developing an analogous model where the tower geometry is simplified on purpose to conform to a multi-degree-of-freedom mechanical model and (2) deriving the equivalent properties of ideal elements where mass stiffness and damping coefficients of idealized elements are derived from the geometry of the tower.

4.3.1 Developing an Analogous Model

The wind turbine tower consists of complex geometrical non-linearities (e.g., flange connections, welded joints, door opening and stiffeners, interior equipment...) that demand attention for a proper design. Accounting said factors in can be achieved by developing a finite element model for each design candidate and comparing their behaviors under loading with respect to the reference model. Application of this approach is costly in terms of time and resources due to the nature of finite element analysis. Therefore, developing a quantitative means to assess the feasibility of a given parameter set beforehand serves a crucial purpose in fatigue studies.

To simplify the description of behavior of the tower, the geometrical non-linearities must be neglected. This results in a single body to work with. The model can be simplified further by employing lumped-element model where the spatially distributed properties can be described by lumped ideal elements. The tower can be divided into lumped masses, connected by massless passive elements. Increasing the amount of lumped

mass that is used increases the accuracy of the model since this configuration yields to a closer approximation to distributed mass model. The representation of such a system is shown in figure 4.7.

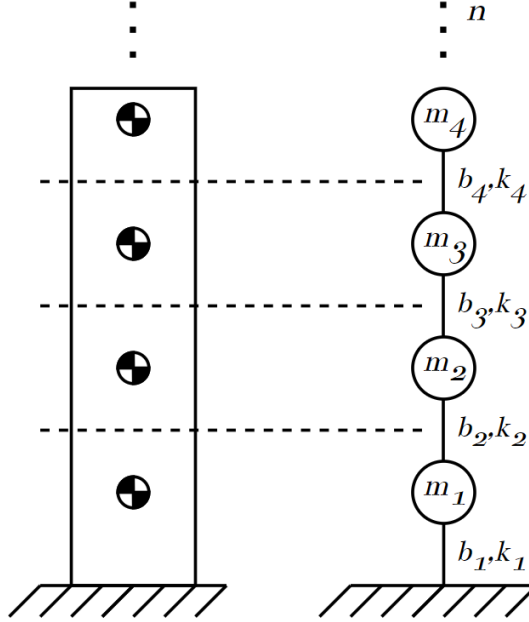


Figure 4.7: Lumped-parameter system analogous to the tower.

The position of the lumped masses are bound by their elevation from ground and the angular deflection from the normal axis. Given some non-zero initial condition, the relation between the angular deflection and horizontal displacement can be established, provided that the deflection angle is sufficiently small. The analogous translational mechanical system is developed from the linearization of the equation of motion.

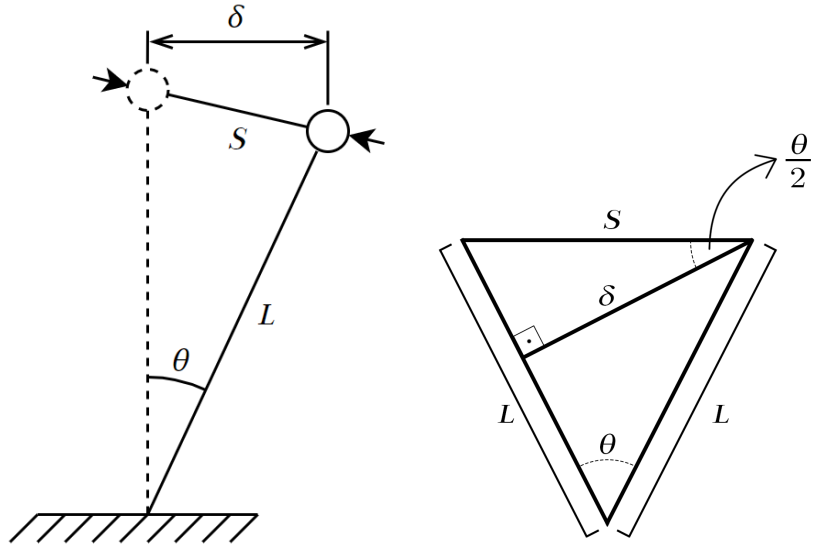


Figure 4.8: Geometrical the relation between the horizontal deflection and true deflection.

Comparing horizontal deflection δ with the true deflection S shown in fig. 4.8,

$$S \cos \frac{\theta}{2} = \delta \quad (4.43)$$

$$\lim_{\theta \rightarrow 0} \left(\cos \frac{\theta}{2} \right) = \frac{\delta}{S} \therefore \delta = S \text{ for small deflection angles} \quad (4.44)$$

Therefore, analogous translational mechanic system model is projected to conform with the rotational mechanical system model for relatively small angles. The error can be represented as the difference of the horizontal deflection and the true deflection. Since given dynamic loads result in extremely small deflection angles, it is safe to assume that the true deflection can be estimated by a translational mechanical system model shown in figure 4.9.

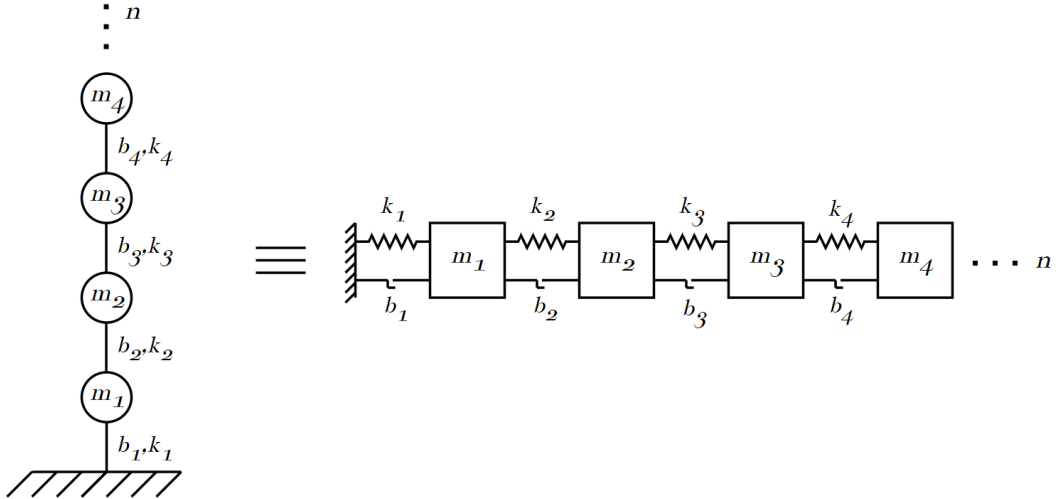


Figure 4.9: Translational mechanical system representation of the lumped-parameter system.

Equation of motion:

$$\begin{bmatrix} m_1 & \dots & 0 \\ \vdots & \ddots & \vdots \\ 0 & \dots & m_n \end{bmatrix} \begin{bmatrix} \ddot{x}_1 \\ \vdots \\ \ddot{x}_n \end{bmatrix} = \begin{bmatrix} b_1 & \dots & 0 \\ \vdots & \ddots & \vdots \\ 0 & \dots & b_n \end{bmatrix} \begin{bmatrix} \dot{x}_1 \\ \vdots \\ \dot{x}_n \end{bmatrix} + \begin{bmatrix} k_1 & \dots & 0 \\ \vdots & \ddots & \vdots \\ 0 & \dots & k_n \end{bmatrix} \begin{bmatrix} x_1 \\ \vdots \\ x_n \end{bmatrix} \quad (4.45)$$

Solving for the undamped eigenmodes of the system:

$$\det \left(\begin{bmatrix} k_1 & \dots & 0 \\ \vdots & \ddots & \vdots \\ 0 & \dots & k_n \end{bmatrix} - \omega^2 \begin{bmatrix} m_1 & \dots & 0 \\ \vdots & \ddots & \vdots \\ 0 & \dots & m_n \end{bmatrix} \right) = 0 \quad (4.46)$$

Where ω are the eigenfrequencies of the system.

To develop the state space of the system, linear graph approach can be used. Additionally, an ideal force source acting on each lumped mass is assumed.

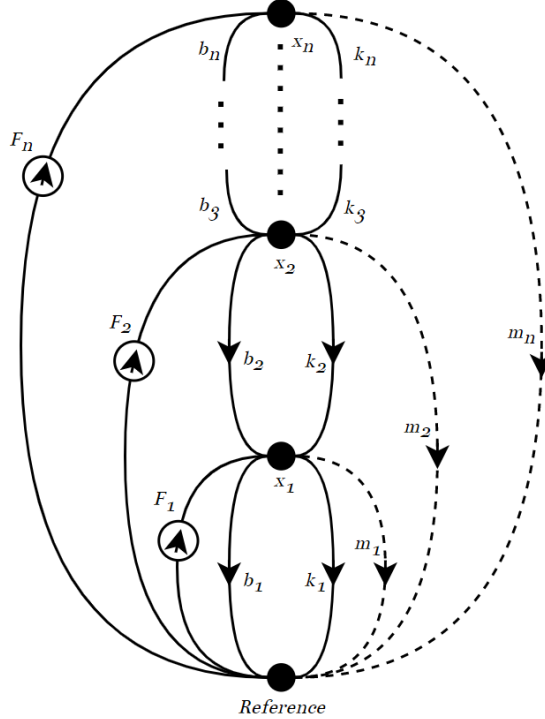


Figure 4.10: Linear graph representation of the translational system shown in 4.9.

Since the analysis regards the positions of the lumped masses, state space variables can be chosen to be the position and the velocity of each lumped mass. In that case, the size of the state vector becomes $2n \times 1$ as shown in equation 4.47.

$$[x] = \begin{bmatrix} x_1 \\ \dot{x}_1 \\ x_2 \\ \dot{x}_2 \\ \vdots \\ x_n \\ \dot{x}_n \end{bmatrix} \quad (4.47)$$

To develop the state and input matrices of the system, continuity equations spanning from the n^{th} node to 1^{st} node can be written in terms of the position of the mass. To generalize this process, only three continuity equations are sufficient; 1^{st} node, 2^{nd} node and n^{th} node since from the 2^{nd} node, all intermediate node equations can be inferred.

1^{st} node continuity equation:

$$F_1(t) - m_1 \ddot{x}_1 - b_1 \dot{x}_1 - k_1 x_1 + b_2 (\dot{x}_2 - \dot{x}_1) + k_2 (x_2 - x_1) = 0 \quad (4.48)$$

$$\ddot{x}_1 = \frac{F_1(t)}{m_1} - \frac{b_1}{m_1}\dot{x}_1 - \frac{k_1}{m_1}x_1 + \frac{b_2}{m_1}(\dot{x}_2 - \dot{x}_1) + \frac{k_2}{m_1}(x_2 - x_1) \quad (4.49)$$

$$\ddot{x}_1 = \frac{F_1(t)}{m_1} - \frac{k_1 + k_2}{m_1}x_1 - \frac{b_1 + b_2}{m_1}\dot{x}_1 + \frac{k_2}{m_1}x_2 + \frac{b_2}{m_1}\dot{x}_2 \quad (4.50)$$

n^{th} node continuity equation:

$$F_n(t) - m_n\ddot{x}_n - b_n(\dot{x}_n - \dot{x}_{n-1}) - k_n(x_n - x_{n-1}) = 0 \quad (4.51)$$

$$\ddot{x}_n = \frac{F_n(t)}{m_n} - \frac{b_n}{m_n}(\dot{x}_n - \dot{x}_{n-1}) - \frac{k_n}{m_n}(x_n - x_{n-1}) \quad (4.52)$$

$$\ddot{x}_n = \frac{F_n(t)}{m_n} + \frac{k_n}{m_n}x_{n-1} + \frac{b_n}{m_n}\dot{x}_{n-1} - \frac{k_n}{m_n}x_n - \frac{b_n}{m_n}\dot{x}_n \quad (4.53)$$

2^{nd} node continuity equation:

$$F_2(t) - m_2\ddot{x}_2 - b_2(\dot{x}_2 - \dot{x}_1) - k_2(x_2 - x_1) + b_3(\dot{x}_3 - \dot{x}_1) + k_3(x_3 - x_2) = 0 \quad (4.54)$$

$$\ddot{x}_2 = \frac{F_2(t)}{m_2} - \frac{b_2}{m_2}(\dot{x}_2 - \dot{x}_1) - \frac{k_2}{m_2}(x_2 - x_1) + \frac{b_3}{m_2}(\dot{x}_3 - \dot{x}_2) + \frac{k_3}{m_2}(x_3 - x_2) \quad (4.55)$$

$$\ddot{x}_2 = \frac{F_2(t)}{m_2} + \frac{k_2}{m_2}x_1 + \frac{b_2}{m_2}\dot{x}_1 - \frac{k_2 + k_3}{m_2}x_2 - \frac{b_2 + b_3}{m_2}\dot{x}_2 + \frac{k_3}{m_2}x_3 + \frac{b_3}{m_2}\dot{x}_3 \quad (4.56)$$

To develop intermediate continuity equations, indexing state variables based on their element number on the state vector can be utilized. This way, the 2^{nd} node continuity equation can be generalized for every intermediate node between 1 and n.

$$\ddot{x}_n = \frac{F_n(t)}{m_n} + \frac{k_n}{m_n}x_{n-1} + \frac{b_n}{m_n}\dot{x}_{n-1} - \frac{k_n + k_{n+1}}{m_n}x_n - \frac{b_n + b_{n+1}}{m_n}\dot{x}_n + \frac{k_{n+1}}{m_n}x_{n+1} + \frac{b_{n+1}}{m_n}\dot{x}_{n+1} \quad (4.57)$$

The equations shown above can be generalized for a system having m nodes as below:

$$\ddot{x}_n = \begin{cases} -\frac{k_n+k_{n+1}}{m_n}x_n - \frac{b_n+b_n}{m_n}\dot{x}_n + \frac{k_{n+1}}{m_n}x_{n+1} + \frac{b_{n+1}}{m_n}\dot{x}_{n+1} + \frac{F_n(t)}{m_n}, & n = 1 \\ \frac{k_n}{m_n}x_{n-1} + \frac{b_n}{m_n}\dot{x}_{n-1} - \frac{k_n+k_{n+1}}{m_n}x_n - \frac{b_n+b_{n+1}}{m_n}\dot{x}_n + \frac{k_{n+1}}{m_2}x_{n+1} + \frac{b_{n+1}}{m_2}\dot{x}_{n+1} + \frac{F_n(t)}{m_n}, & m > n > 1 \\ \frac{k_n}{m_n}x_{n-1} + \frac{b_n}{m_n}\dot{x}_{n-1} - \frac{k_n}{m_n}x_n - \frac{b_n}{m_n}\dot{x}_n + \frac{F_n(t)}{m_n}, & n = m \end{cases} \quad (4.58)$$

For given tower geometry, each section of the tower can be thought of as a point mass including the masses of adjacent flanges and its corresponding shell. Additional to that, the rotor nacelle assembly must also be added in. Diagram illustrating such system is shown in figure 4.11.

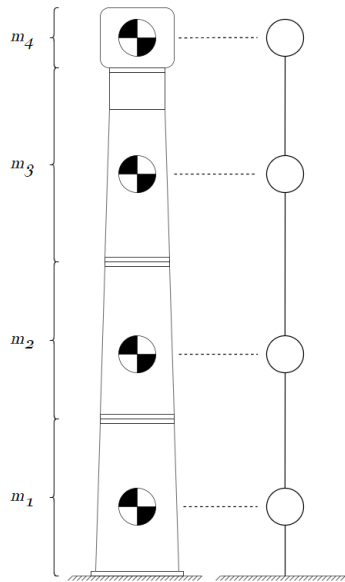


Figure 4.11: Diagram masses on the tower geometry including flanges.

The equivalent translational mechanical system in this case includes 4 translational masses connected with ideal spring and damper elements as discussed prior.

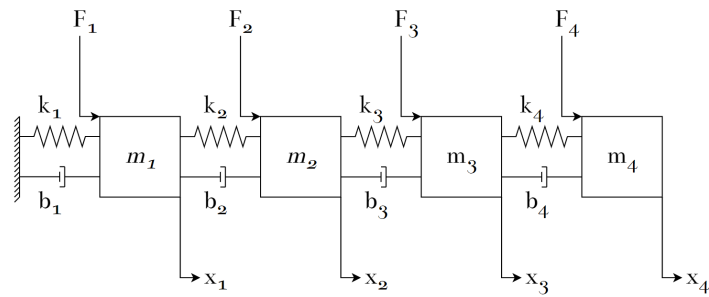


Figure 4.12: Diagram of the translational mechanical system.

$$\begin{bmatrix} \dot{x}_1 \\ \ddot{x}_1 \\ \dot{x}_2 \\ \ddot{x}_2 \\ \dot{x}_3 \\ \ddot{x}_3 \\ \dot{x}_4 \\ \ddot{x}_4 \end{bmatrix} = \begin{bmatrix} 0 & 1 & 0 & 0 & 0 & 0 & 0 & 0 \\ -(k_1+k_2)/m_1 & -(b_1+b_2)/m_1 & k_2/m_1 & b_2/m_1 & 0 & 0 & 0 & 0 \\ 0 & 0 & 0 & 1 & 0 & 0 & 0 & 0 \\ k_2/m_2 & b_2/m_2 & -(k_2+k_3)/m_2 & -(b_2+b_3)/m_2 & k_3/m_2 & b_3/m_2 & 0 & 0 \\ 0 & 0 & 0 & 0 & 0 & 1 & 0 & 0 \\ 0 & 0 & k_3/m_3 & b_3/m_3 & -(k_3+k_4)/m_3 & -(b_3+b_4)/m_3 & k_4/m_3 & b_4/m_3 \\ 0 & 0 & 0 & 0 & 0 & 0 & 1 & 0 \\ 0 & 0 & 0 & 0 & k_4/m_4 & b_4/m_4 & -k_4/m_4 & -b_4/m_4 \end{bmatrix} \begin{bmatrix} x_1 \\ x_2 \\ x_3 \\ x_4 \\ \dot{x}_1 \\ \dot{x}_2 \\ \dot{x}_3 \\ \dot{x}_4 \end{bmatrix} + \begin{bmatrix} 0 & 0 & 0 & 0 \\ 1/m_1 & 0 & 0 & 0 \\ 0 & 0 & 0 & 0 \\ 0 & 1/m_2 & 0 & 0 \\ 0 & 0 & 0 & 0 \\ 0 & 0 & 1/m_3 & 0 \\ 0 & 0 & 0 & 0 \\ 0 & 0 & 0 & 1/m_4 \end{bmatrix} \begin{bmatrix} F_1 \\ F_2 \\ F_3 \\ F_4 \end{bmatrix}$$

Let output equal to the state vector:

$$y = Ix \quad (4.59)$$

The transfer functions of the system are developed as following:

$$\dot{x} = Ax + Bu \quad (4.60)$$

$$y = Ix \quad (4.61)$$

$$\mathcal{L}\{\dot{x}\} = \mathcal{L}\{Ax + Bu\} \quad (4.62)$$

$$sX - x(0) = AX + BU \quad (4.63)$$

$$\mathcal{L}\{y\} = \mathcal{L}\{Ix\} \quad (4.64)$$

$$Y = X \quad (4.65)$$

$x(0)$ is the initial condition for the point masses. Let $x(0) = 0$:

$$sX - AX = BU \quad (4.66)$$

$$X = (sI - A)^{-1} BU \quad (4.67)$$

Therefore, the transfer function becomes

$$\begin{bmatrix} F_1x_1 & F_2x_1 & F_3x_1 & F_4x_1 \\ F_1v_1 & F_2v_1 & F_3v_1 & F_4v_1 \\ F_1x_2 & F_2x_2 & F_3x_2 & F_4x_2 \\ F_1v_2 & F_2v_2 & F_3v_2 & F_4v_2 \\ F_1x_3 & F_2x_3 & F_3x_3 & F_4x_3 \\ F_1v_3 & F_2v_3 & F_3v_3 & F_4v_3 \\ F_1x_4 & F_2x_4 & F_3x_4 & F_4x_4 \\ F_1v_4 & F_2v_4 & F_3v_4 & F_4v_4 \end{bmatrix} = \begin{bmatrix} s & -1 & 0 & 0 & 0 & 0 & 0 & 0 \\ (k_1 + k_2) / m_1 & s + ((b_1 + b_2) / m_1) & -k_2 / m_1 & -b_2 / m_1 & 0 & 0 & 0 & 0 \\ 0 & 0 & s & -1 & 0 & 0 & 0 & 0 \\ -k_2 / m_2 & -b_2 / m_2 & (k_2 + k_3) / m_2 & s + ((b_2 + b_3) / m_2) & -k_3 / m_2 & -b_3 / m_2 & 0 & 0 \\ 0 & 0 & 0 & 0 & s & -1 & 0 & 0 \\ 0 & 0 & -k_3 / m_3 & -b_3 / m_3 & (k_3 + k_4) / m_3 & s + ((b_3 + b_4) / m_3) & -k_4 / m_3 & -b_4 / m_3 \\ 0 & 0 & 0 & 0 & 0 & 0 & s & -1 \\ 0 & 0 & 0 & 0 & -k_4 / m_4 & -b_4 / m_4 & k_4 / m_4 & s + (b_4 / m_4) \end{bmatrix}^{-1} \begin{bmatrix} 0 & 0 & 0 & 0 \\ 1 / m_1 & 0 & 0 & 0 \\ 0 & 0 & 0 & 0 \\ 0 & 1 / m_2 & 0 & 0 \\ 0 & 0 & 0 & 0 \\ 0 & 0 & 1 / m_3 & 0 \\ 0 & 0 & 0 & 0 \\ 0 & 0 & 0 & 1 / m_4 \end{bmatrix}$$

4.3.2 Deriving Equivalent Ideal Elements

After a simplified system describing the behavior of the tower is established, the coefficients of the ideal elements can be obtained through the geometry of the tower. As previously mentioned, geometrical non-linearities are excluded in this process as well. This lets necessary calculations to be proceeded for radially symmetric bodies. To refer to a certain part of the tower, shell and flanges are represented by an index number, shown in table 4.8.

No.	Type	Description
1	Flange	Upper flange
2	Shell	Azimuth shell
3	Shell	Upper section shell
4	Flange	Upper-intermediate connection flange 1
5	Flange	Upper-intermediate connection flange 2
6	Shell	Intermediate section shell
7	Flange	Intermediate-lower connection flange 1
8	Flange	Intermediate-lower connection flange 2
9	Shell	Lower section shell
10	Flange	Base flange

Table 4.8: Parts of the tower and their corresponding indices.

The convenience of using such a notation is significant when calculating equivalent stiffness and damping coefficients, since the point where the point mass is assigned divides the shell element unevenly. Three properties that are aimed to be obtained are mass, stiffness and damping coefficient.

Mass

Mass of a given body is proportional with its volume. Describing the volume of the body by given design parameters (see section 4.1.1)

$$M_i = \rho V_i \quad (4.68)$$

For the tower design, lower and intermediate sections include a shell element and 2 adjacent flanges while the top section includes an additional shell (azimuth shell). The point masses are calculated as

$$m_1 = \sum_{i=8}^{10} M_i, \quad m_2 = \sum_{i=5}^7 M_i, \quad m_3 = \sum_{i=1}^4 M_i, \quad m_4 = \frac{F_{RNA}}{g} \quad (4.69)$$

The stiffness of a body describes the resistance of an elastic body to deform under the presence of force, therefore it is directly related with the strain energy concept.

Stiffness

The stiffness of elements in the case of this study is calculated using strain energy method, also referred as the Castigliano's Theorem. The theorem states that the displacement of a linear elastic system can be determined based on the partial derivatives of the energy [22].

Applying unit load to the body, the resulting displacement δ is calculated by Castigliano's second theorem using the following formulation.

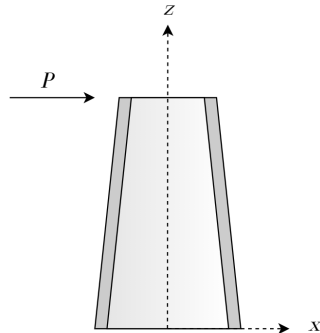


Figure 4.13: Diagram of the bending of one section within the Castigliano's second theorem calculation.

$$S_i = \delta_i^{-1} \text{ for } P = 1N \quad (4.70)$$

$$\delta_i = \frac{\partial}{\partial P} \int_0^{h_i} \frac{M_i^2(z)}{2EI_i} dz \quad (4.71)$$

$$I_i = \frac{\pi}{4} \left(\left(\frac{D_i + t_i \sqrt{g_i^2 + 1}}{2} \right)^4 - \left(\frac{D - t_i \sqrt{g_i^2 + 1}}{2} \right)^4 \right) \quad (4.72)$$

$$M_i = Pz \quad (4.73)$$

Equations 4.70 through 4.73 are solved using MATLAB symbolic toolbox. The result is referred to at section 4.2.1.

As seen in the figure 4.14, the point mass connections divide shells unevenly from their respective center of mass (CoM) points. An equivalent stiffness in this case can be derived, assuming that the rate of change of deflection at any given point on the body is proportional with its vertical distance. Separating the body by a given distance, x , is an approach similar to cutting a spring from a given point. The problem can be solved by said analogy as follows.

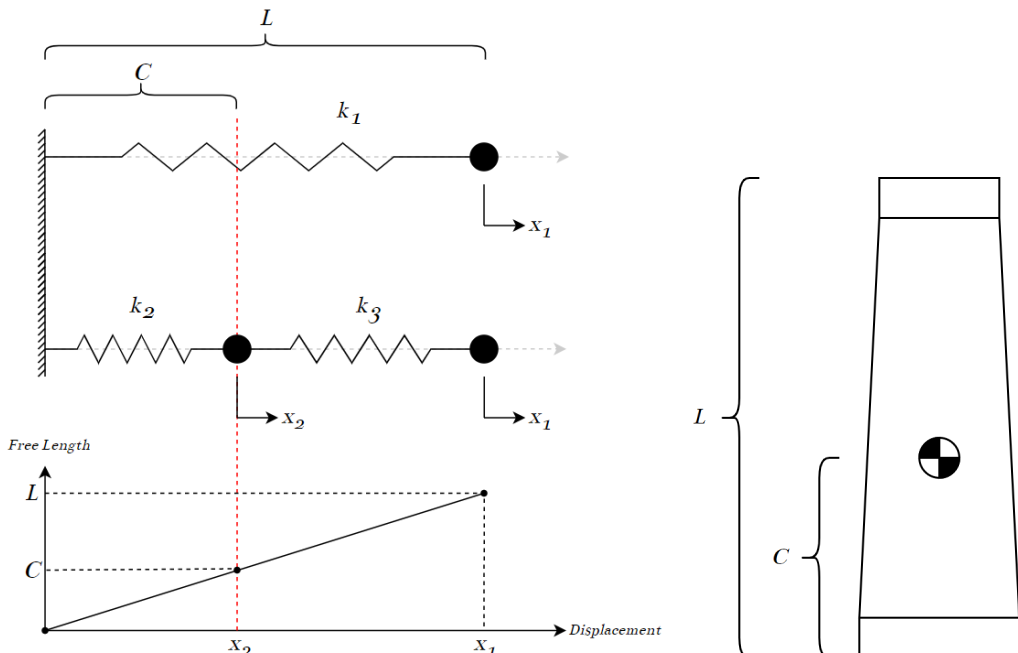


Figure 4.14: Spring element analogous of a shell section.

$$k_1 = (k_2^{-1} + k_3^{-1})^{-1} \quad (4.74)$$

$$\frac{L}{x_1}x_2 = C, \quad \therefore x_2 = \frac{Cx_1}{L} \quad (4.75)$$

$$f = k_1 x_1 = k_2 x_2 \quad (4.76)$$

$$k_1 = k_2 \frac{C}{L}, \quad \therefore k_2 = \frac{k_1 L}{C} \quad (4.77)$$

Substituting k_2 to equation 4.74:

$$k_1 = \left(\frac{C}{Lk_1} + \frac{1}{k_3} \right)^{-1} \quad (4.78)$$

$$k_1 = \frac{Lk_1 k_3}{Ck_3 + Lk_1} \quad (4.79)$$

$$\therefore k_3 = \frac{Lk_1}{L - C} \quad (4.80)$$

The formulation is applied to the tower case where the center of mass of each section is referred as CoM₁, CoM₂, CoM₃ and CoM₄, and the individual stiffness values of parts are referred to as S.

$$k_1 = \left[S_{10}^{-1} + \left(S_9 \left(\frac{h_9}{\text{CoM}_1 - h_{10}} \right) \right)^{-1} \right]^{-1} \quad (4.81)$$

$$k_2 = \left[\left(S_9 \left(\frac{h_9}{h_{10} + h_9 - \text{CoM}_1} \right) \right)^{-1} + S_8^{-1} + S_7^{-1} + \left(S_6 \left(\frac{h_6}{\text{CoM}_2 - \sum_7^{10} h_i} \right) \right)^{-1} \right]^{-1} \quad (4.82)$$

$$k_3 = \left[\left(S_6 \left(\frac{h_6}{\sum_6^{10} h_i - \text{CoM}_2} \right) \right)^{-1} + S_5^{-1} + S_4^{-1} + \left(S_3 \left(\frac{h_3}{\text{CoM}_3 - \sum_4^{10} h_i} \right) \right)^{-1} \right]^{-1} \quad (4.83)$$

$$k_4 = \left[\left(S_3 \left(\frac{h_3}{\sum_3^{10} h_i - \text{CoM}_3} \right) \right)^{-1} + S_2^{-1} + S_1^{-1} \right]^{-1} \quad (4.84)$$

Damping

The damping coefficient of a linear elastic body describes its ability to dissipate energy while subjected to loads. In a system dynamics framework, this ability is described by ideal dissipative elements shown as dampeners. Corresponding damping ratio of the dampener can vary based on the assumptions that are made. In the case of the dynamic study, the damping ratio of a body is assumed to be an inherent characteristic of the system and a constant damping coefficient of $\zeta = 0.05$ is assumed, as it is corroborated by various literature on given tower material and geometry [ref!!!!]. As previously done on mass and stiffness calculations, the damping coefficient of each part of the tower is calculated separately as follows.

$$F(t) = \ddot{x} + \frac{b}{m}\dot{x} + \frac{k}{m}x \quad (4.85)$$

Characteristic equation:

$$F(t) = \ddot{x} + 2\zeta\omega_n\dot{x} + \omega_n^2x \quad (4.86)$$

$$\omega_n = \sqrt{\frac{k}{m}}, \quad 2\zeta\omega_n = \frac{b}{m} \quad (4.87)$$

$$\therefore b = 2\zeta\sqrt{km} \quad (4.88)$$

A similar formulation with stiffness can be used to derive the damping ratio of each element. As seen in equation 4.92, the individual damping values of parts are referred to as B .

$$b_1 = \left[B_{10}^{-1} + \left(B_9 \left(\frac{h_9}{\text{CoM}_1 - h_{10}} \right) \right)^{-1} \right]^{-1} \quad (4.89)$$

$$b_2 = \left[\left(B_9 \left(\frac{h_9}{h_{10} + h_9 - \text{CoM}_1} \right) \right)^{-1} + B_8^{-1} + B_7^{-1} + \left(B_6 \left(\frac{h_6}{\text{CoM}_2 - \sum_7^{10} h_i} \right) \right)^{-1} \right]^{-1} \quad (4.90)$$

$$b_3 = \left[\left(B_6 \left(\frac{h_6}{\sum_6^{10} h_i - \text{CoM}_2} \right) \right)^{-1} + B_5^{-1} + B_4^{-1} + \left(B_3 \left(\frac{h_3}{\text{CoM}_3 - \sum_4^{10} h_i} \right) \right)^{-1} \right]^{-1} \quad (4.91)$$

$$b_4 = \left[\left(B_3 \left(\frac{h_3}{\sum_3^{10} h_i - \text{CoM}_3} \right) \right)^{-1} + B_2^{-1} + B_1^{-1} \right]^{-1} \quad (4.92)$$

4.3.3 Damage Accumulation

IEC 61400-1 recommends that the wind speed distribution over long periods be represented by either the Rayleigh or the Weibull distribution. Our methodology uses the Weibull distribution, with Weibull parameters k and λ chosen arbitrarily from measurements made within the IZTECH campus [23], the graph of which is shown in figure 4.15. There exist methods in literature with which Weibull parameters at an arbitrary hub height can be estimated, which would yield a more realistic probability density function (PDF). The values obtained are for the northerly winds, which are dominant for chosen data by a wide margin. Under normal circumstances, data acquisition regarding candidate locations precedes WT design. This methodology is constructed in a way such that it is applicable to any wind data and hub height. Additionally, if it is found that the wind direction is irregular at a location, it can be accounted for with an added PDF of wind direction.

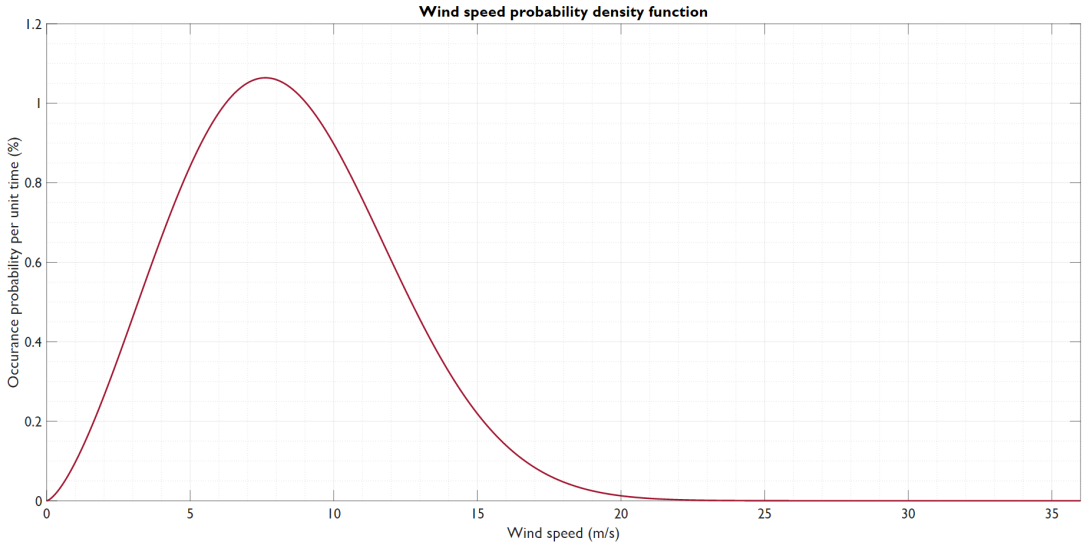


Figure 4.15: Probability density function of the wind speed, expressed as a Weibull distribution with $k = 2.47$ and $\lambda = 9.4$.

The Weibull distribution is mathematically expressed as follows.

$$f(x; \lambda, k) = \frac{k}{\lambda} \left(\frac{x}{\lambda} \right)^{k-1} e^{-(x/\lambda)^k} \text{ for all } x \geq 0 \quad (4.93)$$

Where λ and k are the scale and shape parameters respectively. The variable x , in this case, represents the wind speed.

4.4 Defining the Cost Function

The design variables which are optimized based on mass minimization are correlated to cost of the tower. The reduction on the cost, which is targeted for least 5%, is quantifiable and directly related to design changes.

There are several processes that predominantly determine the cost, such as welding, bending, cutting cost, etc. There are also additional costs such as shipping and assembling. In our methodology, these type costs are not factored in, due to their relatively low effect on the total cost. The cost functions outlined in this section are similar to those proposed by Farkas et al. [17]. The constituent parameters of the cost function is illustrated in figure 4.16 and equation 4.94.

$$K = K_M + K_{F0} + K_{F1} + K_{F2} + K_{F3} + K_P \quad (4.94)$$



Figure 4.16: The constituent parameters of the cost function.

Material Cost

The total amount of material used is correlated with the volume of the tower. As shell sections and flanges are assumed to be of the same material, the function can be expressed with equation 4.95.

$$K_M = k_M \rho V_{\text{total}} \quad (4.95)$$

Where k_M is the material cost factor, assumed 1\$ per kilogram, ρ is the density of the material, and V_{total} is given in 4.19.

Forming Cost

The forming cost of each shell element is represented as K_{F0} , and can be expressed with equation 4.96.

$$K_{F0} = k_F \theta_F T \quad (4.96)$$

Where T is the operation time for a 3m wide sheet steel. T can be calculated using 4.97 for sheets with thicknesses and rolling radii of $4\text{mm} \leq t \leq 40\text{mm}$, and $1750\text{mm} \leq t \leq 3500\text{mm}$. The equation also factors in the imperfections caused by the forming process. θ_F is the difficulty factor, which takes into account the difficulty of the process. It is taken as 3, in accordance to the literature. k_F is the labor cost factor for each unit time, and is assumed to be 1\$/min.

$$\ln T = 6.85825 - 4.5272t_n^{-0.5} + 0.0095419D_n^{0.5} \quad (4.97)$$

Each segment has a specific number of shell elements of approximately 3m in height. This value is subject to change in order to accommodate new design proposals. The reference model has 4 shell elements for the lower and the intermediate sections, and 5 shell elements for the upper section.

Welding Cost

The shell sections are connected together with full penetration butt welds, longitudinally and circumferentially, as shown in figure 4.17.

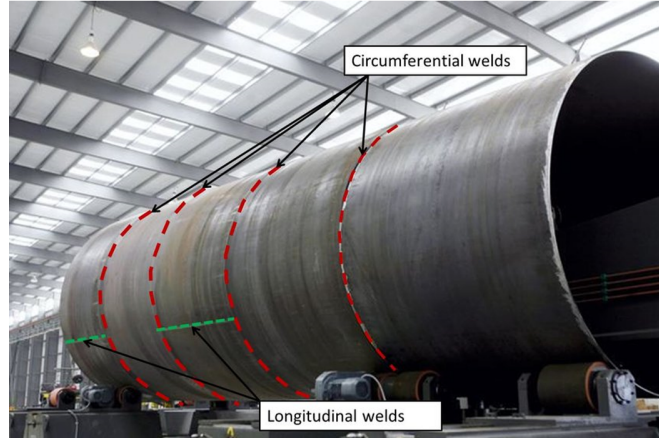


Figure 4.17: Welding regions on the edges of shell elements [24]

The cost of longitudinal welds, K_{F1} is represented by equation 4.98.

$$K_{F1} = k_F \left(\theta_W \sqrt{\kappa \rho V_n} \right) + k_F [1.3 \cdot 0.224 \cdot 10^{-3} t_n^2 (3000 \kappa)] \quad (4.98)$$

Where θ_W is the difficulty factor, which is used to factor in the complexity of the assembly. It is taken as 2 in accordance with the literature. κ is the number of structural part that is assembled, which is 2, and n is the number of shell element in a given segment. V_n is the volume of the n^{th} shell element of a given segment, and is represented by equation 4.100.

$$V_n = \pi t_i h_n (D_n - g_i h_n) \sqrt{g_i^2 + 1} \quad (4.99)$$

$$h_n = \frac{H_i}{n} \quad (4.100)$$

$$D_{n+1} = D_n - 2g_i h_n \quad (4.101)$$

Where t_i , g_i and H_i are the thickness, growth rate and height of the i^{th} shell element respectively. The welding cost for circumferential welds, K_{F2} as seen in figure 4.17 for each segment is calculated as with equation 4.102.

$$K_{F2} = k_F \left(\theta_W \sqrt{n \cdot n \rho V_n} \right) + 1.3 \cdot 0.2245 \cdot 10^{-3} t_n^2 \cdot 4\pi D_n \quad (4.102)$$

Cutting Cost

The cost of cutting for each shell element, K_{F3} is represented by equation 4.103.

$$K_{F3} = k_F \theta_C C_c t_n^{0.25} L_c \quad (4.103)$$

Where θ_C is the difficulty factor, which is taken as 3 in accordance with the literature. C_c is the cutting parameter and equals 1.1388×10^{-3} . L_c is the approximate cutting length for each shell element, which is calculated by the following equation.

$$L_c = D_n + (D_n - 2g_i h_n) + 2h_n \tan^{-1} g_i \quad (4.104)$$

Painting Cost

The cost of painting for each shell element, K_P is represented by equation 4.105.

$$K_P = k_p S_p \quad (4.105)$$

Where k_p is the paint cost factor, which is taken as 14.4×10^{-6} \$/mm². S_p is the surface area of the tower to be painted, which is calculated as shown in equation 4.106.

$$S_p = \frac{\pi (D_i + (D_i - 2g_i H_i)) H_i}{2} \quad (4.106)$$

4.5 Finite Element Analysis

A cursory inspection of the reference tower geometry reveals complexities that cannot be practically reflected via any analytical approach. In problems with complex geometries, boundary conditions and loads, a mathematical model is generated and solved numerically using FEA software. One such software, Ansys, was used in assessing the static and dynamic responses of the tower in this project, in addition to harmonic analyses.

The FEA analyses are set up following the important factors in section 3.6. A parameterized FEA model is created, with the parameters reflecting the ones determined in 4.1.1. This allows for rapid iteration of the FEA model, cutting down on the time required for modeling. At earlier stages, optimization via FEA using response surface methodology was considered, but due to computational intensity, the focus of the study shifted to analytical optimization.

Engineering judgement should be exercised in assessing the results. Validation tests are helpful in ascertaining the accuracy of the relation between initial conditions and the results.

The center of the combined RNA weight was calculated by the following equation.

$$x_w = \frac{\sum_{i=1}^n w_i x_i}{w_i} \quad (4.107)$$

Where x_w is the position vector of i^{th} point mass with relation to the global origin. The point masses included are the 3 blades, the hub, and the nacelle. The resultant point mass was multiplied with the gravitational acceleration to obtain a point load.

In figure 4.18, the results of the quasi-static analyses of the reference and proposed designs in the conditions of 36 and 52 m/s wind as stipulated by IEC.

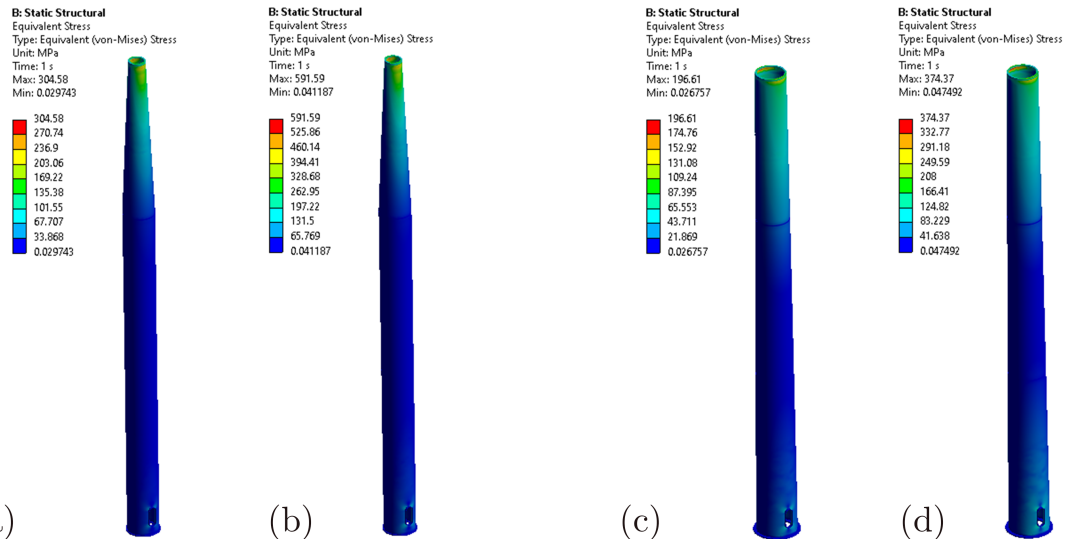


Figure 4.18: The quasi-static analysis results of: (a) Reference tower at 36 m/s wind, (b) Reference tower at 52 m/s wind, (c) Proposed tower at 36 m/s wind, (d) Proposed tower at 36 m/s wind.

Since this step in the analysis is linear, the maximum stress values that happen to be above the yield strength of the material are no cause for concern, as they are restricted to a few nodes that in reality would yield somewhat, due to the ductility of the material used.

4.5.1 Modal Analysis

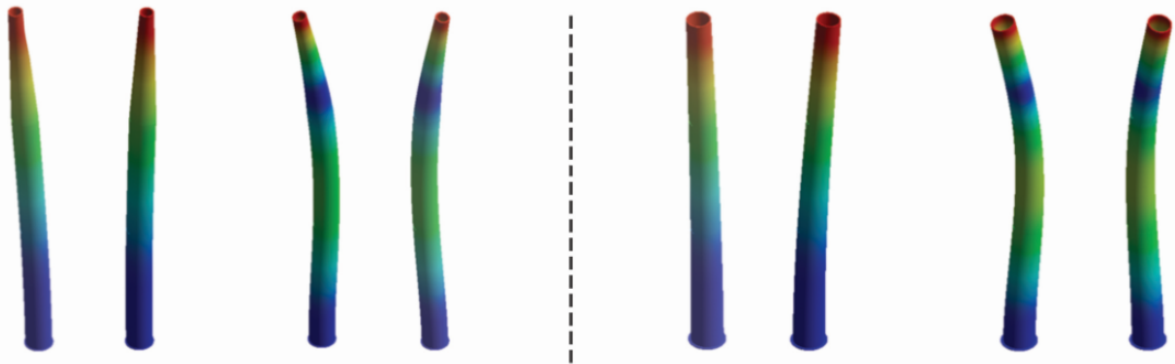


Figure 4.19: The 1st and 2nd eigenfrequencies (fore-aft, side-to-side respectively) of the reference (left) and the proposed (right) designs.

The literature showed that the fasteners connecting the flanges together can also be points of failure. While it is computationally infeasible to model every detail of the system (such as the threaded bolts), there are ways of simplifying the analysis and saving computation time. One such simplification is modeling the bolt and the inside of the nut as plain surfaces, and using *bonded connections* within the FEA program. This adds a boundary condition that makes it so that the adjacent nodes on the contacting surfaces cannot move or rotate in any axis with relation to one another. This process is shown in figure 4.20.

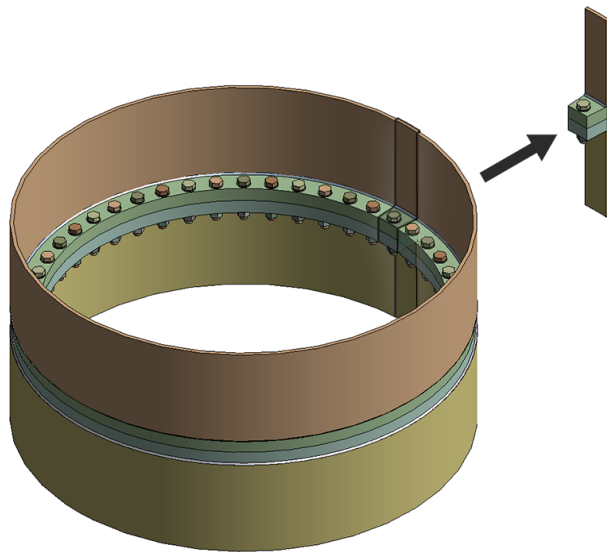


Figure 4.20: A partial model is obtained from a full model of the flange connection.

The flanges rely on the friction caused by the pre-tension of the bolt in the fastener assembly, plus the weight of the tower, to maintain contact with one another. The Ansys

analogous to this behaviour is a frictional connection. The mesh model of the partial model is shown in figure 4.21.

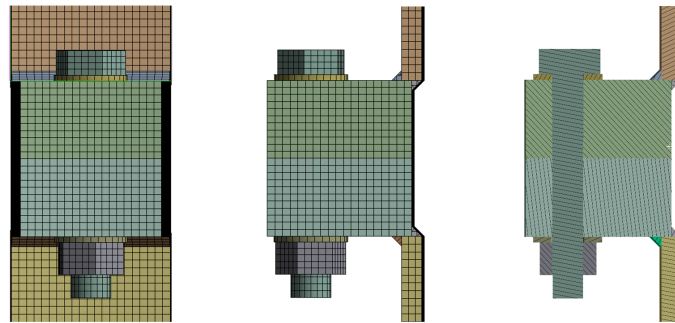


Figure 4.21: Left-to-right: A close-up view of the fastener mesh from the front, the side, and cross-section view.

It was decided later in the project that this section of the analyses are the hardest to properly represent the real-life counterpart of, and was therefore not fully carried out in the interest of time.

4.6 Comparison of the Analytical and the FEA methods

Although it is not reasonable to make quantitative statements about the feasibility of the model using FEA in a project with a scope such as this one, it was shown that the FEA analyses are in general agreement with the results anticipated from the outcomes of the analytical study, with the exception of the added information, such as the geometrical non-linearities, and stress concentrations that arise from said non-linearities.

Results and Discussion

In this chapter, the research and analysis results are obtained using the methods described in chapter 4 in a systematic way. First, the loads acting on the tower are calculated as an input for the design optimization and validation studies. The calculated forces also provide a well-defined baseline for a reasonable comparison between the reference and proposed models. In the following sections, the results are given in three sections, which are the outcomes of the optimization, analytical dynamic and FEA studies as constructed in chapter 4.

5.1 Load Calculation

All the required inputs to calculate the loads acting on the tower are given in section 4.1.4. Contributions of each force component is given below.

The wind loads (W_w) on each section of the tower are shown in table 5.1.

Section	W_w (N/m)
1	4714.3
2	5428.0
3	4228.8

Table 5.1: Calculated values for different values of height, z [9].

All static loads described in section 4.1.4 are listed in table 5.2.

Term	Direction	Unit	Value
W_w	x	N/m	5.1
W_t	$-z$	N	300470
F_T	x	N	139810
M_T	y	Nm	248030
F_{RNA}	$-z$	N	253294
M_{RNA}	y	Nm	289610

Table 5.2: All of the calculated loads and moments for the wind speed of 36 m/s.

Also, the tower should be considered for the survival condition where the wind speed

is 52 m/s with a braked (static) rotor. The loads and moments are shown for the survival condition in table 5.3.

Term	Direction	Unit	Value
W_w	x	N/m	Sec. 1: 9.8361×10^3 Sec. 2: 11.325×10^3 Sec. 3: 8.8231×10^3
W_T	$-z$	N	300470
F_T	x	N	139810
M_T	y	Nm	248030
F_{RNA}	$-z$	N	253294
M_{RNA}	y	Nm	289610

Table 5.3: All of the calculated loads and moments for the wind speed of 52 m/s.

The dynamic forces at a given wind speed is represented using the amplitude and the frequency of the force. Since the functions representing those are developed continuously, the amplitude and frequency of the dynamic forces can be plotted against the wind speed.

In the case of rotor and blade forces, both the amplitude and the frequency graph is the same for both models. The results for blade and rotor forces are shown in figures 5.1 and 5.2.

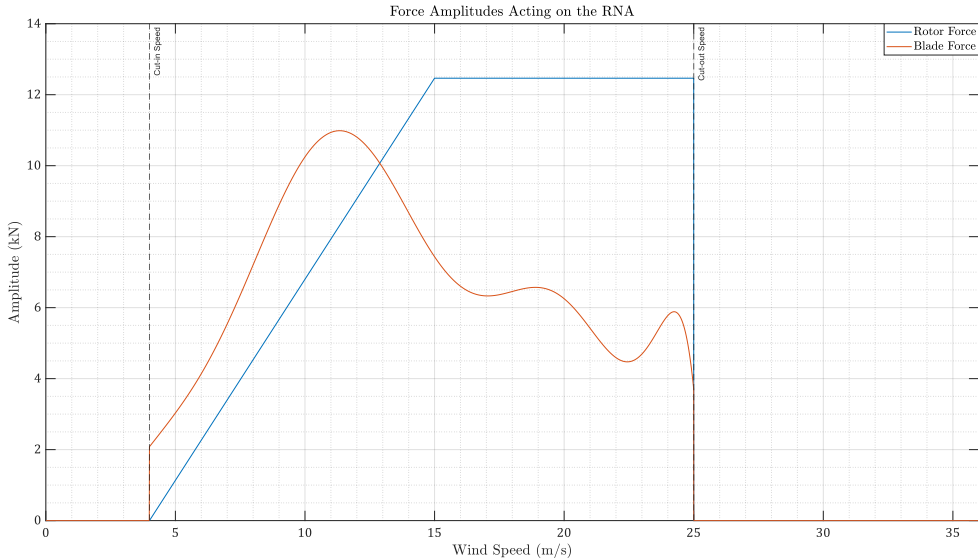


Figure 5.1: Force amplitudes acting on the RNA.

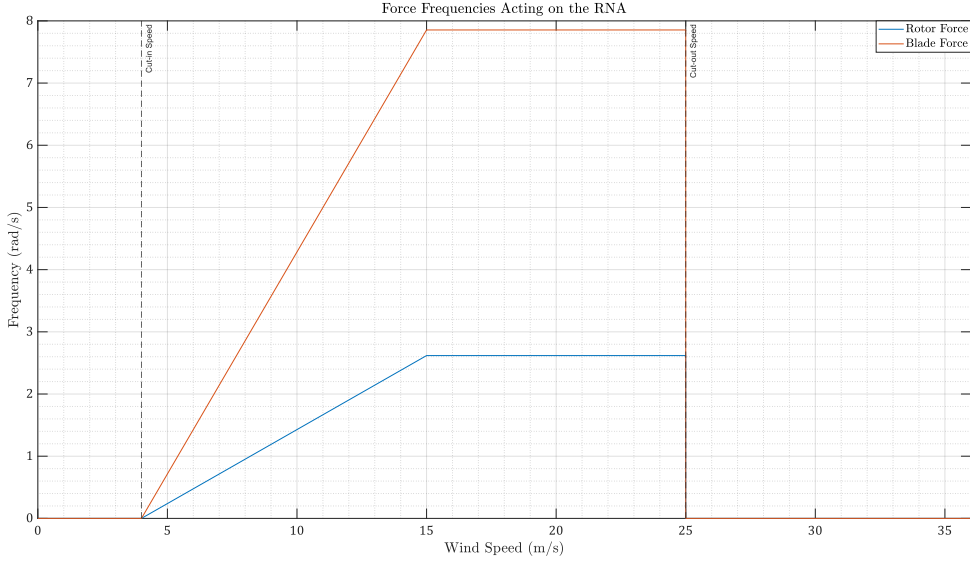


Figure 5.2: Force frequencies acting on the RNA.

As seen from the figures, the effect of the rotor and blade forces are in effect within the interval of cut-in and cut-out speeds.

Remaining dynamic forces are dependant on the geometry of the sections as well as the tower. The force amplitudes of the vortex shedding force for reference and proposed designs are shown in fig figures 5.3 and 5.4.

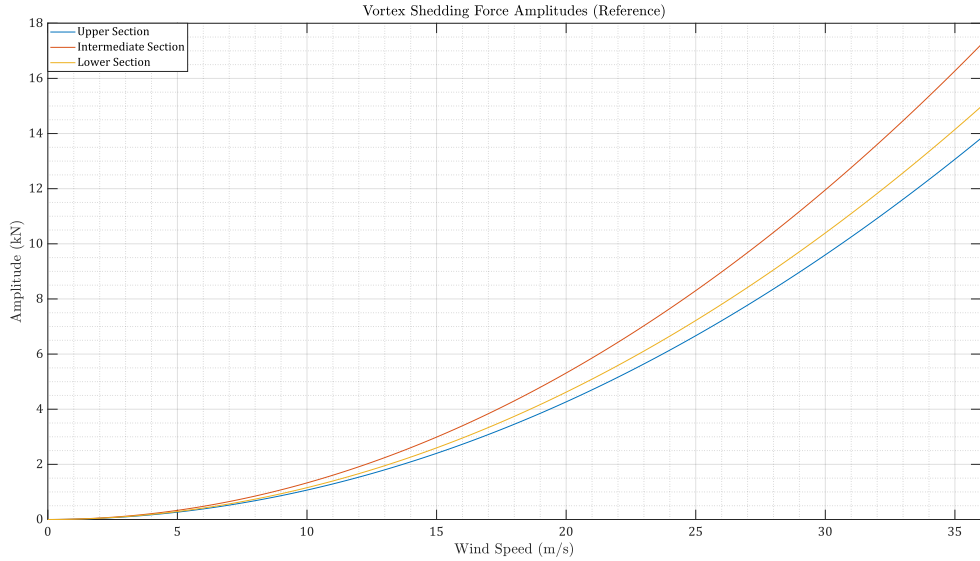


Figure 5.3: Vortex shedding force amplitudes of the reference tower.

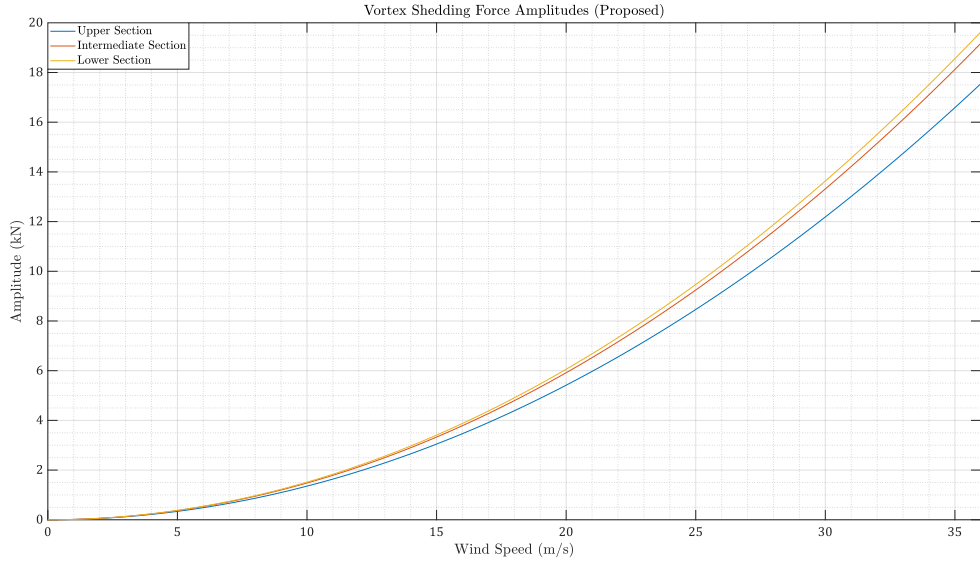


Figure 5.4: Vortex shedding force amplitudes of the proposed design.

Since the outer diameter of the proposed design is larger compared to the reference design (see table 5.6), consequently the surface area interacting with the wind is larger. This results in higher vortex shedding amplitudes for the proposed design. The vortex shedding frequency of the reference and proposed design is shown in figures 5.5 and 5.6 respectively:

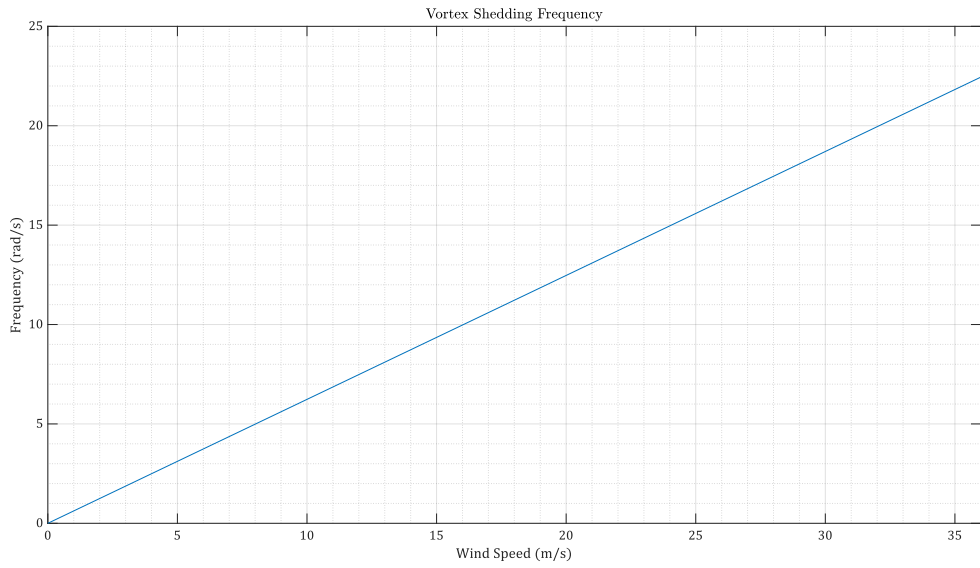


Figure 5.5: Vortex shedding force amplitudes of the reference tower.

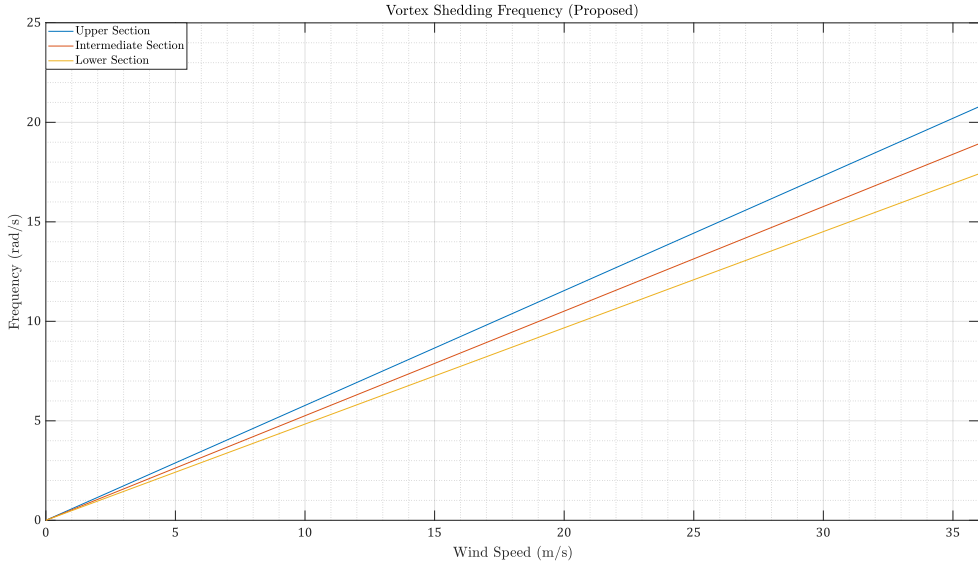


Figure 5.6: Vortex shedding force amplitudes of the proposed design.

The vortex shedding frequency is dependant on the outer diameter of the tower. For tower sections with a non-zero growth rate, this fact causes a problem, since there is no definitive vortex shedding frequency, but an interval spanning from values corresponding to maximum and minimum outer diameters of the section. Therefore, the lower outer diameter of the sections are considered to be the vortex shedding frequency which result in distinguishable peaks in deflection graphs (see x). In reality, these peaks are not present and can be thought of as the maximum value that the deflection curve might reach. This artifact is due to the limitations of the lumped-element model, and can be reduced by increasing the degree of freedom of the model by adding more point masses.

5.2 Optimization Results

In order to perform a successful design optimization of a wind turbine tower, the following are considered:

- Loads acting on the tower (see: 4.4)
- Design parameters (see: 4.1.1)
- Design constraints (see: 4.1.2)
- Assumptions (see: 4.1.3)
- Objective function derived based on optimization strategy (see: 4.2.1)

By taking the listed items into account above, a proper optimization solver is selected from Matlab Optimization Toolbox as `fmincon`. The rest of the section shows the results based on the static analysis of the proposed design and its comparison with the reference

model. The design parameter set of the proposed design is given table 5.4 and the solid model which is created based on the proposed design parameters and its representative view are given in figure 5.7, along with the reference model for comparison.

Design Parameters		
Symbol	Reference	Proposed
H_1	12.03	12.77
H_2	12.04	11.83
H_3	11.3	10.76
t_1	0.018	0.012
t_2	0.018	0.011
t_3	0.015	0.010
g_1	0	0.0089
g_2	0	0.0099
g_3	0.0426	0.0109
D_1	2.2	2.85

Table 5.4: Parameters of the reference tower and the proposed design.

Although the proposed design parameters are the outcomes of an iterative process of the `fmincon` function in MATLAB, it is still critical to understand the reasoning behind the evolution of the new design parameter set by meticulously thinking about the effects of the design constraints introduced. This way, the correlations between the reference and proposed model can be understood fully. The lowest stiffness value belongs the third segment of the reference tower, due to its smaller overall diameter and larger height. In the proposed model, the segment height is reduced and the section diameter is increased to achieve a higher stiffness value in the third section. This way, the overall stiffness of the tower is significantly increased. Thus, the shell thicknesses could be reduced for each segment such that the stiffness still tends to improve due to the dominant effect of the diameter increase. Moreover, the introducing growth rates to the first and second segments proved to be a very effective way of reducing the mass further while increasing the stiffness. the literature research revealed that introducing the growth rate in each section is widely accepted method for mass reduction. By using the proposed parameters, considerable improvements in the tower mass and cost are obtained. The total mass (including both shell elements and flanges) is reduced by 16.7% and the total cost decreases by 21.4%. Table 5.5 shows cost reductions of each production process for both the reference and proposed models.

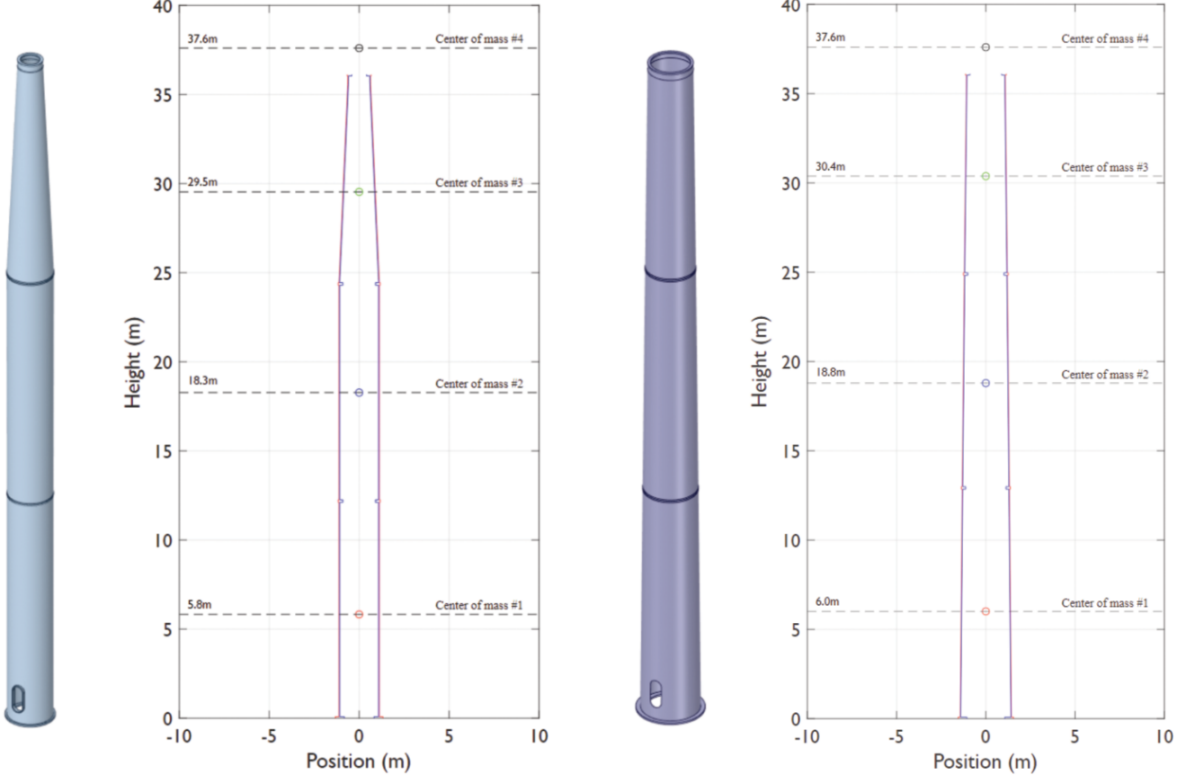


Figure 5.7: The comparison of geometries of the reference (left) and proposed model (right).

Cost factor	Material (K_m)	Forming (K_{F0})	Welding (K_{F1})	Welding (K_{F2})	Cutting (K_{F3})	Painting (K_P)	Total (K)
Reference	33815\$	18948\$	8249\$	5354\$	1829\$	2216\$	70412\$
Proposed	28154\$	15199\$	4292\$	3070\$	1882\$	2725\$	55322\$
Change	-16.7%	-19.8%	-47.9%	-42.7%	+2.9%	+22.9%	-21.4%

Table 5.5: The cost comparison between the reference and proposed models.

The material cost is reduced significantly due to the reduction in the volume of the tower. Despite the increase in the tower's diameter, the forming cost decreases as well, since the decrease in the thickness affects the forming cost more dominantly than the diameter, due to the fact that thinner metal sheets are easier to roll. Besides that, considerable decrements are observed in welding costs due to their direct relationship between the thickness and volume of the tower. On the other hand, the cutting cost increases since the cutting length gets larger due to the increase in the total diameter of the tower. Also, the painting cost rises severely due to remarkable surface area increment of the tower caused by the increase in the total diameter. However, the contribution of the painting cost is relatively low in the total cost. Eventually, the total cost is reduced by 21.4% by using proposed design parameters. The saving in the cost should not affect the

service life adversely. Based on the design criterion, the service life should be maintained at least when the cost reduction is the target. Therefore, the improvements in tower properties that are directly related to the design criteria (cost & service life) are given in table 5.6.

Comparison of Reference and Proposed Design Properties				
Property	Unit	Reference	Proposed	Change (%)
Mass	kg	33722	28099	-16.67
Production cost	\$	70412	55322	-21.43
Equivalent stiffness	kN/m	7738.3	9190.7	18.77
Equivalent damping	kNs/m	1.53	1.51	-0.85
Excitatory wind speed	m/s	23.1	27.4	18.61
Natural frequency	Hz	2.28	2.51	10.09
Maximum deflection	mm	41	38	-7.32

Table 5.6: Comparison of properties of the reference tower and the proposed design.

Although analytical static studies provide a comprehensive model about the wind turbine tower, it is based on several assumptions and simplifications to make it more manageable for the MATLAB Optimization methods. Increasing the complexity and completeness of the models in this phase leads to an inefficient computation power usage. Therefore, further detailed validation regarding the life service and stress calculations are considered in the next two sections, namely analytical dynamic studies and FE studies.

5.3 Dynamic Study Results

The dynamic study yields the transfer function of the analogous model and based on that, the frequency response of the reference and proposed designs can be inferred from the bode magnitude diagrams. The two points of interest are the 1st and 2nd eigenmodes of the model which correspond to feasible wind speeds that may occur in nature. These points are calculated for the undamped case (see section 4) and varies from the results discussed for FE studies. Said discrepancy is expected due to the simplified nature of the lumped-element model, however, a comparative evaluation between two models can safely be made.

The bode magnitude diagrams of the reference and proposed designs is given in figures 5.8 and 5.9.

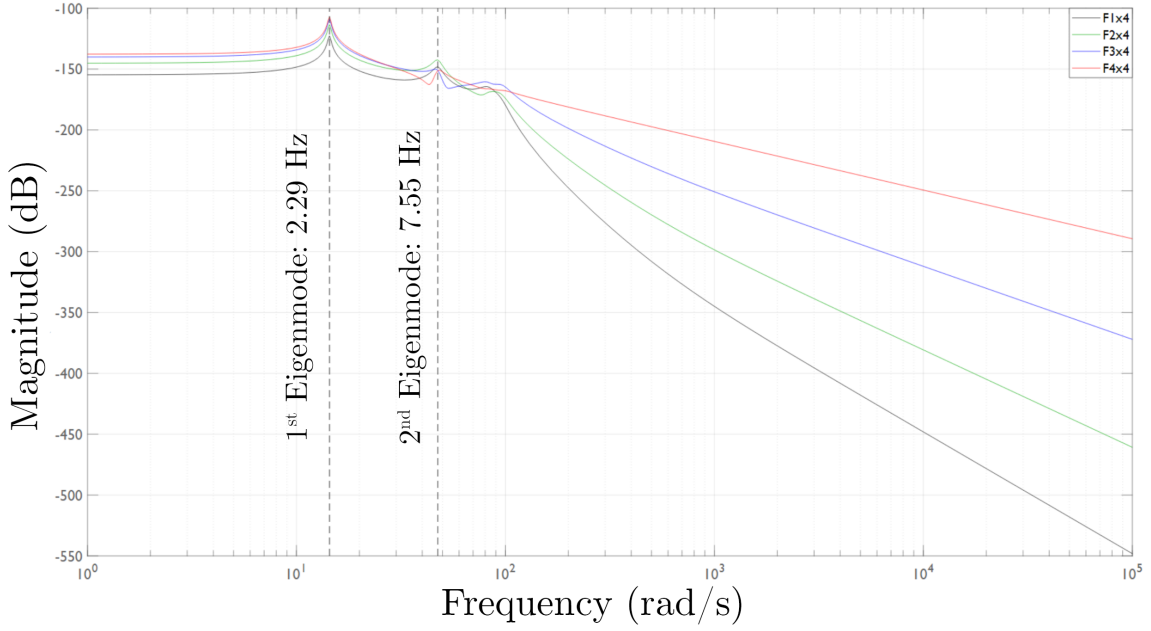


Figure 5.8: The bode magnitude diagram of the reference tower.

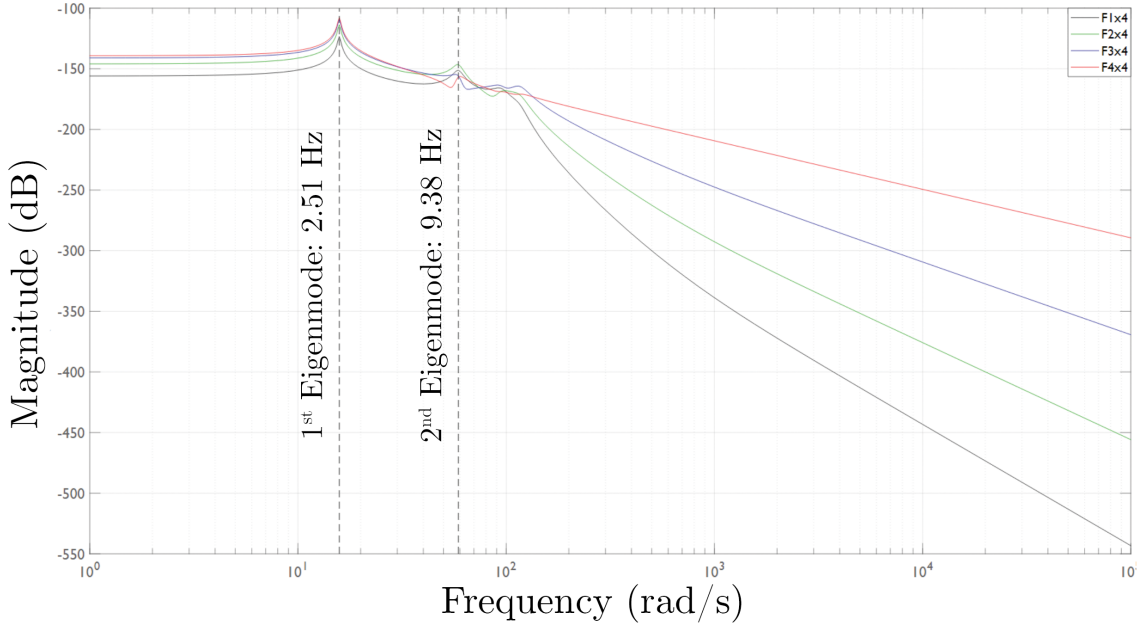


Figure 5.9: The bode magnitude diagram of the proposed design.

As seen from the bode diagrams, the 1st eigenfrequency of the proposed design is at a higher frequency value compared to the reference tower. The reason of this change can be explained by the increase in stiffness compared to the reference design. There is no significant difference between the excitation magnitudes of both systems, meaning that the 0.85% reduction in damping of proposed design does not affect the behaviour of the tower negatively. Another point of comparison between two designs are the tip

point deflections at a given wind speed. These cannot be directly predicted from the bode diagrams of the designs since the amplitudes and the frequencies of applied dynamic loads also change with the geometry of the design (see section dynamic loads methodology). The tip point deflections calculated from the applied dynamic forces and the transfer functions of both designs are shown in figures 5.10 and 5.11 as follows.

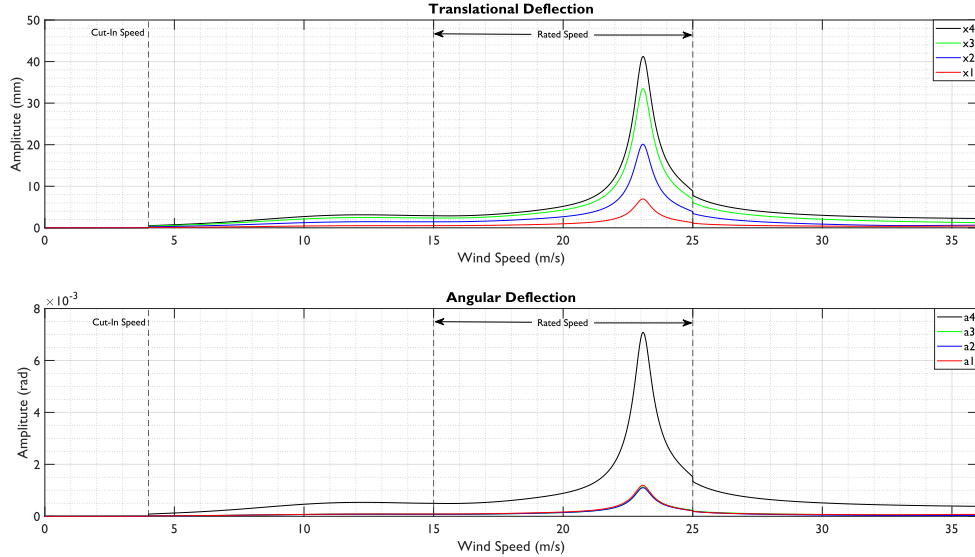


Figure 5.10: The tip point deflection graph of the reference tower.

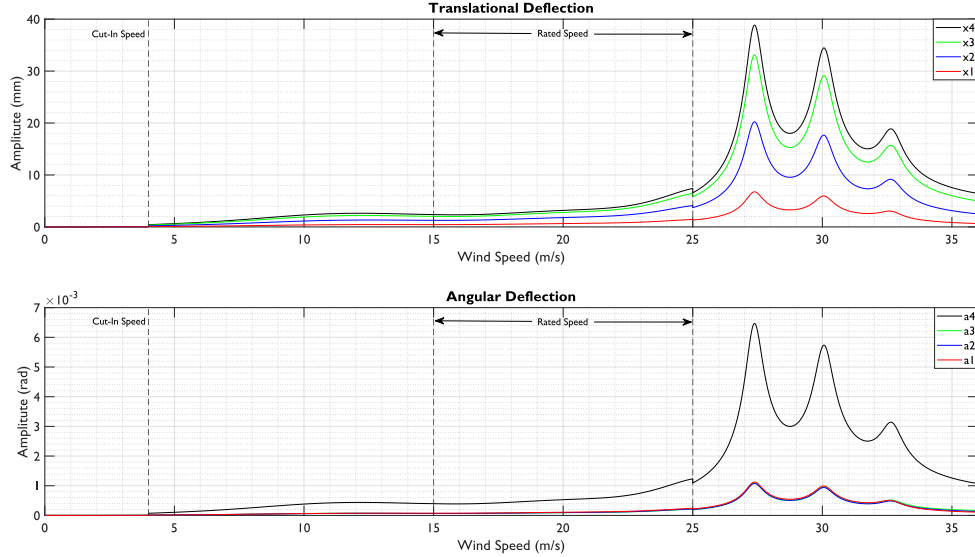


Figure 5.11: The tip point deflection graph of the proposed design.

The excitatory wind speeds are the peaks in figures 5.10 and 5.11 and are projected to cause the highest amount of damage compared to deflections at other frequencies. By

increasing the outer diameter and therefore the stiffness of the tower, the eigenfrequencies of the design have increased alongside with a significant decrease in the slope of the vortex shedding frequencies with respect to the wind speed, resulting in a more desirable behaviour within the interval of rated speed. Furthermore, the increase in excitatory wind speed also implies that the tower is projected to experience these frequencies considerably less (see figure 4.15).

5.4 Further Studies

5.4.1 Detailed Cost Analysis

In order for any power production method to be profitable, total energy produced over the plant's life cycle compared to its installation, operation and maintenance expenditures should be greater than other alternative energy production methods with similar energy potential. This is often compared by the leveled cost of energy (LCOE), which is the measure of the average net cost of electricity generation in current, normalized prices.

The leveled cost of energy is given as:

$$LCOE = \frac{\text{sum of the costs over lifetime}}{\text{sum of electrical energy produced over lifetime}} = \frac{\sum_{t=1}^N \frac{I_t + M_t + F_t}{(1+r)^t}}{\sum_{t=1}^N \frac{E_t}{(1+r)^t}} \quad (5.1)$$

Where:

I_t : Investment expenditures in year t

M_t : Operation and maintenance expenditures in year t

F_t : Additional expenditures in year t

E_t : Electrical energy generated in the year t

r : Discount rate

n : Expected lifetime of the power plant

The LCOE represents the cost of electricity from the producer's standpoint. The discount rate accounts for the factors such as government subsidies and social cost of capital. LCOE of a wind turbine is given as follows [25].

$$LCOE = \left(\frac{ICC \cdot FCR}{AEP} \right) + O\&M \quad (5.2)$$

Where financial parameters; ICC (Installed Capital Cost):

$$LCOE = \left(\frac{ICC \cdot FCR}{AEP} \right) + O\&M \quad (5.3)$$

OCC (Overnight Capital Cost):

$$OCC = TCC + BOS + SC \quad (5.4)$$

TCC (Turbine Capital Cost)

BOS: (Balance of Plant Cost)

SC: (Soft Costs: insurance + contingency + decommissioning)

$$\text{insurance} \approx (TCC + BOS) \cdot 0.02, \quad \text{contingency} \approx (TCC + BOS) \cdot 0.1 \quad (5.5)$$

CF: (Construction Financing)

AEP: (Annual Energy Production)

FCR: (Fixed Charge Rate)

O&M: (Operation and Maintenance)

For the purpose of a cost study of a WT, some values of parameters are often assumed based on the region that the wind turbine is proposed to be built in. It is often possible to derive a rough estimation of LCOE on a per-plant basis using historical relations and data from industry.

5.4.2 Connections and the Foundation

Further research must be made in order to obtain a comprehensive estimation with regards to the fatigue life of the bolts in the ring-flange connection. Veljkovic et al. have exhaustively documented the process of bolt-connection analysis in wind turbine towers [5].

Additionally alternative methods of connections in place of ring-flange connections can be investigated, such as the solutions developed under High Strength Tubular Tower For Wind Turbines (HISTWIN) project [26]. These connections have been shown to have superior fatigue properties and cheaper to manufacture, for a total decrease of the tower cost by around 10%.

Finally, the design or analysis of the foundation of the tower is a fundamental step for the cases in which the tower is designed with the consideration of a seismic region. In such cases, this part of the design cannot be overlooked, as was done in this work.

5.4.3 Stiffeners

Literature has shown that a reliable and relatively inexpensive method of increasing dynamic behaviour of wind turbine towers is the use of internal structures, such as stiffeners [27].

5.5 Finite Element Analysis

Further research into the effect of door opening geometry may be investigated for further improvement. A cursory analysis revealed that the effect that the door opening geometry has with regards to stress concentration is significant, as seen in figure 5.12.

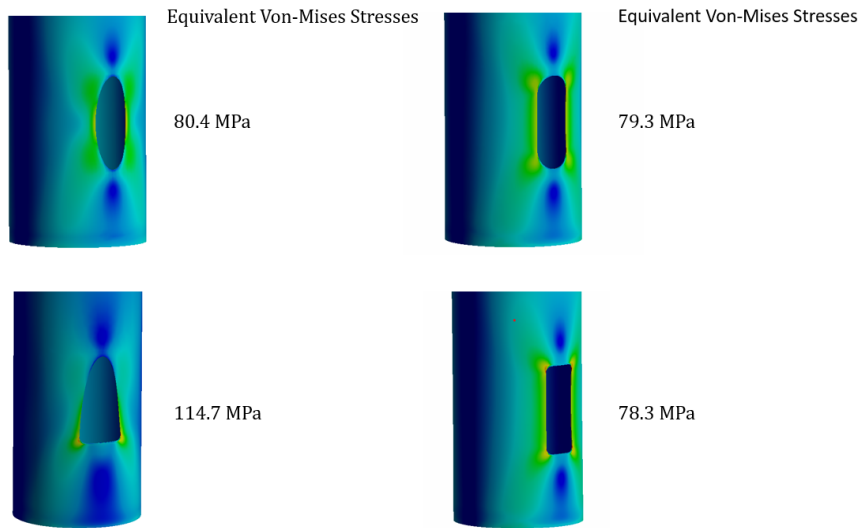


Figure 5.12: The overall methodology for the new design.

Conclusion

In this work, a methodology that utilizes design criteria across static, dynamic, and modal analyses to improve upon a full-scale wind turbine tower was developed. The model is devised as a framework that can be applied to any tower of similar geometry. When applied to the tower provided by our industrial partner, our design yielded a 21.43% reduction in cost, and a 16.67% increase in stiffness. The methodology showed that this reduction in cost did not negatively affect service life. The advantages of the proposed tower geometry are shown to be corroborated by previous research. Devised methodology presented, not only serves a quantitative means to compare the behavior of the wind turbine tower, but also a way to generate set of design parameters that are projected to satisfy given criteria. Wind turbine tower producers may implement prior studies to estimate the static and dynamic behavior of the designed tower efficiently and may compare various design sets based on their costs, mass, and service life.

Bibliography

1. *Renewable energy*, Center for Climate and Energy Solutions. 2021-09. Available also from: [https://www.c2es.org/content/renewable-energy/#:~:text=Wind%5C%20was%5C%20the%5C%20second%5C%20largest,\(707.4%5C%20GW%5C%20is%5C%20onshore\).](https://www.c2es.org/content/renewable-energy/#:~:text=Wind%5C%20was%5C%20the%5C%20second%5C%20largest,(707.4%5C%20GW%5C%20is%5C%20onshore).)
2. *Development of the Cost of Wind-Generated Power*. 2021. Available also from: <https://www.wind-energy-the-facts.org/development-of-the-cost-of-wind-generated-power.html>.
3. *Turbine accident statistics*. 2022-04. Available also from: <https://scotlandagainstspin.org/turbine-accident-statistics/>.
4. FINGERSH, L.; HAND, M.; LAXSON, A. *Wind Turbine Design Cost and Scaling Model*. 2006.
5. VELJKOVIC, M.; FELDMANN, M.; NAUMES, J.; PAK, D.; SIMÕES, L.; DA SILVA; REBELO, C. 9 - Wind turbine tower design, erection and maintenance. In: SØRENSEN, John D.; SØRENSEN, Jens N. (eds.). *Wind Energy Systems*. Woodhead Publishing, 2011, pp. 274–300. Woodhead Publishing Series in Energy. ISBN 978-1-84569-580-4. Available from DOI: <https://doi.org/10.1533/9780857090638.2.274>.
6. ARANY, László; BHATTACHARYA, Subhamoy; MACDONALD, John; HOGAN, S. John. Simplified critical mudline bending moment spectra of offshore wind turbine support structures. *Wind Energy*. 2015, vol. 18, no. 12, pp. 2171–2197. Available from DOI: <https://doi.org/10.1002/we.1812>.
7. NIEBSCH, Jenny; RAMLAU, Ronny; NGUYEN, Thien. Mass and Aerodynamic Imbalance Estimates of Wind Turbines. *Energies*. 2010, vol. 3. Available from DOI: [10.3390/en3040696](https://doi.org/10.3390/en3040696).
8. RICE, Jennifer A.; LAFAVE, James M.; MEHUYS, Christopher H. End Connection Effects on Vortex Shedding Susceptibility of Welded Aluminum Truss Tubular Web Members. *Journal of Performance of Constructed Facilities*. 2008, vol. 22, no. 5, pp. 297–304. Available from DOI: [10.1061/\(ASCE\)0887-3828\(2008\)22:5\(297\)](https://doi.org/10.1061/(ASCE)0887-3828(2008)22:5(297)).
9. NEGM, Hani M.; MAALAWI, Karam Y. Structural design optimization of wind turbine towers. *Computers & Structures*. 2000, vol. 74, no. 6, pp. 649–666. ISSN 0045-7949. Available from DOI: [https://doi.org/10.1016/S0045-7949\(99\)00079-6](https://doi.org/10.1016/S0045-7949(99)00079-6).
10. *Eurocode 3 - Design of steel structures - Part 1-6: Strength and Stability of Shell Structures*. 2007.

11. TRAN, Anh; VELJKOVIC, Milan; REBELO, Carlos; SIMOES, Luis; SILVA, Luís. Buckling Observation of Door Opening for Wind Turbine Towers. In: 2015.
12. *Bolted Joint Design - Fastenal*. Available also from: <https://www.fastenal.com/content/feds/pdf/Article%20-%20Bolted%20Joint%20Design.pdf>.
13. FINGERSH, L.; HAND, M.; LAXSON, A. *Review of small wind turbine construction instructions and specifically for structural supports and foundations*. 2016.
14. *Collapsed wind tower - a root cause investigation*. Element, 2021-05. Available also from: <https://www.element.com/nucleus/2021/collapsed-wind-tower>.
15. PASQUALI, Felipe Meneguzzo. *An Integrative Framework for Optimal Tower Life and Cost*. 2016. PhD thesis. State University of New York at Buffalo.
16. *The Online Materials Information Resource*. Available also from: <https://www.matweb.com/search/datasheet.aspx?matguid=95b1c3e21c734db3b976e0d50389dcc&ckck=1>.
17. UYS, P.E.; FARKAS, J.; JÁRMAI, K.; VAN TONDER, F. Optimisation of a steel tower for a wind turbine structure. *Engineering Structures*. 2007, vol. 29, no. 7, pp. 1337–1342. ISSN 0141-0296. Available from DOI: <https://doi.org/10.1016/j.engstruct.2006.08.011>.
18. *Eurocode 1 - Basis of design and actions on structures - Part 2-1: Actions on structures. Densities, self-weight and imposed loads. ENV 1991-2-1:1999*. 1999.
19. Buckling strength analysis – Classification Notes No. 30.1. *Det Norske Veritas (DNV)*. 2004.
20. *Solver-based nonlinear optimization*. Available also from: https://ch.mathworks.com/help/optim/solver-based-nonlinear-optimization.html?s_tid=CRUX_lftnav.
21. *Solver-Based Nonlinear Optimization Functions*. Available also from: <https://ch.mathworks.com/help/optim/ug/fmincon.html>.
22. [N.d.]. Available also from: <https://engineering.purdue.edu/~ce474/Docs/The%20Theorem%20of%20Least%20Work.pdf>.
23. OZERDEM, B; TURKELI, M. An investigation of wind characteristics on the campus of Izmir Institute of Technology, Turkey. *Renewable Energy*. 2003, vol. 28, no. 7, pp. 1013–1027.
24. STAVRIDOU, Nafsika; EFTHYMIOS, Evangelos; BANIOTOPoulos, Charalampos C. Welded Connections of Wind Turbine Towers under Fatigue Loading: Finite Element Analysis and Comparative Study. *American Journal of Engineering and Applied Sciences*. 2015, vol. 8, no. 4, pp. 489–503. Available from DOI: <10.3844/ajeassp.2015.489.503>.
25. LABORATORY, National Renewable Energy. *Best Practices for Operation and Maintenance of Photovoltaic and Energy Storage Systems; 3rd Edition*. 2018.

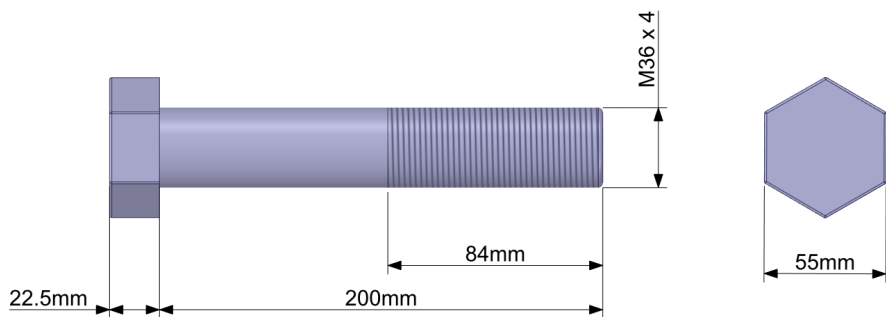
26. VELJKOVIC, Milan; HEISTERMANN, Christine; HUSSON, Wylliam; LIMAM, Marouene; FELDMANN, Markus; NAUMES, J; PAK, Daniel; FABER, Torsten; KLOSE, Marcus; FRUHNER, K-U; KRUTSCHINNA, L; BANIOTOPoulos, Charalampos; LAVASAS, I; PONTES, A; RIBEIRO, E; HADDEN, M; SOUSA, R; SILVA, Luís; REBELO, Carlos; KINNUNEN, H. *High-strength tower in steel for wind turbines (Histwin)*. 2012. ISBN 9789279224348. Available from DOI: 10.2777/39656.
27. DIMOPOULOS, C.A.; GANTES, C.J. Comparison of stiffening types of the cutout in tubular wind turbine towers. *Journal of Constructional Steel Research*. 2013, vol. 83, pp. 62–74. ISSN 0143-974X. Available from DOI: <https://doi.org/10.1016/j.jcsr.2012.12.016>.

Appendix

A.1 Technical Drawings

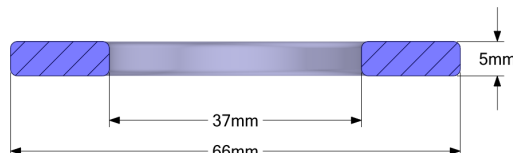
A.1.1 Fastener Parts

DIN931 - M 36 × 200 - 10.9 - KL steel hexagon head bolt



DIN125 - A 37 - A4 steel washer

Inner radius is at minimum and outer radius is at maximum value as stipulated by the standard.



A.2 MATLAB Code

A.2.1 Generating Graphical Results Given Set of Design Parameters

```
1 clc; clear all;
2 initial_parameters = readtable("parameters_init.xlsx");
3 I = table2array(initial_parameters);
4
5
6 % ===== Design Parameters ===== %
7
```

```

8 D = I(:,1); t = I(:,2); g = I(:,3); h = I(:,4);
9
10 % ===== Properties/Conditions ===== %
11
12 Strouhal = 0.22;
13 material_density = 7.8e+3;
14 E = 2.1e+11;
15 damping = 0.05;
16 air_density = 1.25;
17 air_dynamic_viscosity = 1.5e-5*air_density;
18 grav = 9.81;
19 kr = 0.17 * ones(1,10);
20 ct = 1 * ones(1,10);
21 G = 3.5 * ones(1,10);
22 cr = [1.43 1.43 1.43 1.43 1.36 1.36 1.36 1.24 1.24 1.24];
23 cd = 1.1 * ones(1,10);
24 cf = 0.825 * ones(1,10);
25 dynamic_force_factor = 0.25;
26
27 % ===== Mathematical Functions ===== %
28
29 % Volume
30 Volume = @(D,h,g,t) pi .* t .* h .* (D - g .* h) .*...
31     sqrt(g.^2 + 1);
32
33 % Centeroid
34 Centeroid = @(D,h,g) (3.*D.*h.^2 - 4.*g.*h.^3) ./...
35     (6.*D.*h - 6.*g.*h.^2);
36
37 % Moment of Inertia
38 M_I = @(D,g,t) (pi/2)*((D+t.*sqrt(g.^2+1))/2).^4 - ...
39     ((D-t.*sqrt(g.^2+1))/2).^4;
40
41 % Thrust force
42 F_ce = @(cr, ct, kr, g, z) cr.^2 .* ct.^2 .* (1 + 2 .*...
43     g .* (kr ./ (cr .* ct)));
44
45 % Longitudinal cross-sectional area facing wind
46 F_Ac = @(D,t,g,h,z) (D + t.*sqrt(g.^2+1) - g .* (h+z)) .* (h-z);
47
48 % Transverse area
49 F_At = @(D,t,g,z) pi*t.*sqrt(g.^2+1).* (D-2.*g.*z);
50
51 % Weibull distribution
52 wpdf = @(v,w_a,w_k) (w_k./ (w_a.^w_k).* (v.^ (w_k-1)).*...
53     exp(-(v./w_a).^w_k))./100;
54

```

```

55 % ===== 1. Mass ===== %
56
57 V = Volume(D,h,g,t);
58 M = material_density .* V;
59 Ct = Centeroid(D,h,g);
60
61 m1 = sum(M(8:10,:)); % Lower Section Mass (kg)
62 m2 = sum(M(5:7,:)); % Intermediate Section Mass (kg)
63 m3 = sum(M(1:4,:)); % Lower Section Mass (kg)
64 m4 = 289.610e3/9.81; % Assembly Mass (kg)
65
66 % ===== 2. Center of Mass ===== %
67
68 % 1st section
69 CoM1 = (Ct(8:10)' + [sum(h(9:10)) h(10) 0])...
70     *V(8:10)/sum(V(8:10));
71
72 % 2nd section
73 CoM2 = (Ct(5:7)' + [sum(h(6:10)) sum(h(7:10)),...
74     sum(h(8:10))])*V(5:7)/sum(V(5:7));
75
76 % 3rd section
77 CoM3 = (Ct(1:4)' + [sum(h(2:10)) sum(h(3:10)),...
78     sum(h(4:10)) sum(h(5:10))])*V(1:4)/sum(V(1:4));
79
80 % Assembly
81 CoM4 = sum(h) + 1.5;
82
83 % ===== 3. Stiffness Coefficients ===== %
84
85 % Stiffness coefficient vector
86 K = [springcons(D(1),t(1),g(1),h(1),E),...
87     springcons(D(2),t(2),g(2),h(2),E),...
88     springcons(D(3),t(3),g(3),h(3),E),...
89     springcons(D(4),t(4),g(4),h(4),E),...
90     springcons(D(5),t(5),g(5),h(5),E),...
91     springcons(D(6),t(6),g(6),h(6),E),...
92     springcons(D(7),t(7),g(7),h(7),E),...
93     springcons(D(8),t(8),g(8),h(8),E),...
94     springcons(D(9),t(9),g(9),h(9),E),...
95     springcons(D(10),t(10),g(10),h(10),E)];
96
97 % 1st element (Base - lower section connection)
98 k1 = (1/K(10)+(K(9)*(h(9)/Ct(9)))^-1)^-1;
99
100 % 2nd element (Lower - intermediate section connection)
101 k2 = ((K(9)*((h(9)/(h(9)-Ct(9)))))^-1+...

```

```

102 1/K(8)+1/K(7)+(K(6)*(h(6)/Ct(6)))^-1)^-1;
103
104 % 3rd element (Intermediate - upper section connection)
105 k3 = ((K(6)*((h(6)/(h(6)-Ct(6)))))^-1+...
106 1/K(5)+1/K(4)+(K(3)*(h(3)/Ct(3)))^-1)^-1;
107
108 % 4th element (Upper - assembly connection)
109 k4 = ((K(3)*((h(3)/(h(3)-Ct(3)))))^-1+...
110 1/K(2)+1/K(1))^ -1;
111
112 % ===== 4. Damping coefficients ===== %
113
114 % Damping coefficient vector
115 Damp = 2*damping*sqrt(K.*M');
116
117 % 1st element (Base - lower section connection)
118 b1 = (1/Damp(10)+(Damp(9)*(h(9)/Ct(9)))^-1)^-1;
119
120 % 2nd element (Lower - intermediate section connection)
121 b2 = ((Damp(9)*((h(9)/(h(9)-Ct(9)))))^-1+...
122 1/Damp(8)+1/Damp(7)+(Damp(6)*(h(6)/Ct(6)))^-1)^-1;
123
124 % 3rd element (Intermediate - upper section connection)
125 b3 = ((Damp(6)*((h(6)/(h(6)-Ct(6)))))^-1+...
126 1/Damp(5)+1/Damp(4)+(Damp(3)*(h(3)/Ct(3)))^-1)^-1;
127
128 % 4th element (Upper - assembly connection)
129 b4 = ((Damp(3)*((h(3)/(h(3)-Ct(3)))))^-1+...
130 1/Damp(2)+1/Damp(1))^ -1;
131
132
133 % ===== 5. Wind Force Magnitudes (tower) ===== %
134
135 Mag = F_ce(cr, ct, kr, G, h') .* cd .* cf .* F_Ac(D, t, g, h, 0)';
136
137 C1 = sum(Mag(8:10));
138 C2 = sum(Mag(5:7));
139 C3 = sum(Mag(1:4));
140
141 % ===== 5. Natural Frequency ===== %
142
143 % Mass matrix [M]
144 MM(1,1) = m1; MM(2,2) = m2; MM(3,3) = m3; MM(4,4) = m4;
145
146 % Stifness matrix [K]
147 KK(1,:) = [k1+k2 -k2 0 0]; KK(2,:) = [-k2 k2+k3 -k3 0];
148 KK(3,:) = [0 -k3 k3+k4 -k4]; KK(4,:) = [0 0 -k4 k4];

```

```

149
150 syms w
151 DD = det(KK-(w^2).*MM);
152 freq = solve(DD,w);
153
154 % Natural frequencies f (rad/s)
155 f = unique(abs(double(freq)));
156
157 f_hz = f./(2*pi);
158
159 % ===== 6. Frequency Responses & Transfer Functions ===== %
160
161 syms s
162
163 % System matrix [A]
164 A(1,:) = [0 1 0 0 0 0 0 0];
165 A(2,:) = [-(k1+k2)/m1 -(b1+b2)/m1 k2/m1 b2/m1 0 0 0 0];
166 A(3,:) = [0 0 0 1 0 0 0 0];
167 A(4,:) = [k2/m2 b2/m2 -(k2+k3)/m2 -(b3+b2)/m2 k3/m2 b3/m2 0 0 ];
168 A(5,:) = [0 0 0 0 0 1 0 0];
169 A(6,:) = [0 0 k3/m3 b3/m3 -(k3+k4)/m3 -(b4+b3)/m3 k4/m3 b4/m3];
170 A(7,:) = [0 0 0 0 0 0 0 1];
171 A(8,:) = [0 0 0 0 k4/m4 b4/m4 -k4/m4 -b4/m4];
172
173 % Input matrix [B]
174 B(1,:) = [0 0 0 0];
175 B(2,:) = [1/m1 0 0 0];
176 B(3,:) = [0 0 0 0];
177 B(4,:) = [0 1/m2 0 0];
178 B(5,:) = [0 0 0 0];
179 B(6,:) = [0 0 1/m3 0];
180 B(7,:) = [0 0 0 0];
181 B(8,:) = [0 0 0 1/m4];
182
183 % Output matrix [C]
184 C = [1 0 0 0 0 0 0 0;...
185     0 1 0 0 0 0 0 0;...
186     0 0 1 0 0 0 0 0;...
187     0 0 0 1 0 0 0 0;...
188     0 0 0 0 1 0 0 0;...
189     0 0 0 0 0 1 0 0;...
190     0 0 0 0 0 0 1 0;...
191     0 0 0 0 0 0 0 1];
192
193 % Transfer Function Matrix [G]
194 TF = C*((eye(8)*s-A)^-1)*B;
195

```

```

196 % Deflection w.r.t. mass 1 CoM
197 F1x1 = sym2tf(TF(1,1),0); F2x1 = sym2tf(TF(1,2),0);
198 F3x1 = sym2tf(TF(1,3),0); F4x1 = sym2tf(TF(1,4),0);
199
200 % Deflection w.r.t. mass 2 CoM
201 F1x2 = sym2tf(TF(3,1),0); F2x2 = sym2tf(TF(3,2),0);
202 F3x2 = sym2tf(TF(3,3),0); F4x2 = sym2tf(TF(3,4),0);
203
204 % Deflection w.r.t. mass 3 CoM
205 F1x3 = sym2tf(TF(5,1),0); F2x3 = sym2tf(TF(5,2),0);
206 F3x3 = sym2tf(TF(5,3),0); F4x3 = sym2tf(TF(5,4),0);
207
208 % Deflection w.r.t. mass 4 CoM
209 F1x4 = sym2tf(TF(7,1),0); F2x4 = sym2tf(TF(7,2),0);
210 F3x4 = sym2tf(TF(7,3),0); F4x4 = sym2tf(TF(7,4),0);
211
212 % ===== 7. Tower Cross Section Graphical Representation ===== %
213
214 res = 0.001; % resoultion
215 cc = 0; % Index
216
217 D2 = flip(I(:,1)); t2 = flip(I(:,2));
218 g2 = flip(I(:,3)); h2 = flip(I(:,4));
219
220 for i = 1:length(h2)
221     for j = 0:res:h2(i)
222         cc = cc+1;
223         X(1,cc) = (D2(i)/2) + (t2(i) * sqrt((g2(i)^2)+1)) - g2(i)*j;
224         X(2,cc) = (D2(i)/2) - (t2(i) * sqrt((g2(i)^2)+1)) - g2(i)*j;
225     end
226 end
227
228 y = 0:res:res*(cc-1);
229
230 % ===== 8. Tip point deflection amplitute ===== %
231
232 res2 = 0.001;
233 maxwind = 36;
234 windspeed = 0:res2:maxwind;
235
236
237 % 8.1. Rotor and Blade
238
239 rotormag = btf(windspeed) .* (3/16);
240 blademag = btf(windspeed) .* (1/4);
241
242 windrelation = [zeros(1,length(res2:res2:4-res2)), ...

```

```

243 (0:res2:11)./11,ones(1,length(15+res2:res2:25)),...
244 zeros(1,length(25:res2:maxwind))];
```

245

```

246 windrelation2 = [zeros(1,length(res2:res2:4-res2)),...
247 ones(1,length(4:res2:25)),...
248 zeros(1,length(25:res2:maxwind))];
```

249

```

250 rotorfreq = windrelation .* (25*2*pi/60);
251 rotormag = windrelation2 .* rotormag;
```

252

```

253 bladefreq = windrelation .* (25*2*pi/20);
254 blademag = windrelation2 .* blademag;
```

255

```

256 [magrot4,~,~] = bode(F4x4,rotorfreq); MR4(:) = magrot4;
257 [magbl4,~,~] = bode(F4x4,bladefreq); MB4(:) = magbl4;
```

258

```

259 [magrot3,~,~] = bode(F4x3,rotorfreq); MR3(:) = magrot3;
260 [magbl3,~,~] = bode(F4x3,bladefreq); MB3(:) = magbl3;
```

261

```

262 [magrot2,~,~] = bode(F4x2,rotorfreq); MR2(:) = magrot2;
263 [magbl2,~,~] = bode(F4x2,bladefreq); MB2(:) = magbl2;
```

264

```

265 [magrot1,~,~] = bode(F4x1,rotorfreq); MR1(:) = magrot1;
266 [magbl1,~,~] = bode(F4x1,bladefreq); MB1(:) = magbl1;
```

267

268

```

269 % 8.2. Tower
```

270

```

271 qref = air_density .* (windspeed.^2) ./2;
```

272

```

273 lowmag = C1 .* qref .* dynamic_force_factor;
274 intmag = C2 .* qref .* dynamic_force_factor;
275 upmag = C3 .* qref .* dynamic_force_factor;
```

276

```

277 lowfreq = (2*pi*Strouhal/(D(9)+t(9)*sqrt(g(9)^2+1))) .* windspeed;
278 intfreq = (2*pi*Strouhal/(D(6)+t(6)*sqrt(g(6)^2+1))) .* windspeed;
279 upfreq = (2*pi*Strouhal/(D(3)+t(3)*sqrt(g(3)^2+1))) .* windspeed;
```

280

```

281 [maglow4,~,~] = bode(F1x4,lowfreq); ML4(:) = maglow4;
282 [magint4,~,~] = bode(F2x4,intfreq); MI4(:) = magint4;
283 [magup4,~,~] = bode(F3x4,upfreq); MU4(:) = magup4;
```

284

```

285 [maglow3,~,~] = bode(F1x3,lowfreq); ML3(:) = maglow3;
286 [magint3,~,~] = bode(F2x3,intfreq); MI3(:) = magint3;
287 [magup3,~,~] = bode(F3x3,upfreq); MU3(:) = magup3;
```

288

```

289 [maglow2,~,~] = bode(F1x2,lowfreq); ML2(:) = maglow2;
```

```

290 [magint2,~,~] = bode(F2x2,intfreq); MI2(:) = magint2;
291 [magup2,~,~] = bode(F3x2,upfreq); MU2(:) = magup2;
292
293 [maglow1,~,~] = bode(F1x1,lowfreq); ML1(:) = maglow1;
294 [magint1,~,~] = bode(F2x1,intfreq); MI1(:) = magint1;
295 [magup1,~,~] = bode(F3x1,upfreq); MU1(:) = magup1;
296
297 deflection4 = MR4.*rotormag + MB4.*blademag +...
298     ML4.*lowmag + MI4.*intmag + MU4.*upmag;
299 deflection3 = MR3.*rotormag + MB3.*blademag +...
300     ML3.*lowmag + MI3.*intmag + MU3.*upmag;
301 deflection2 = MR2.*rotormag + MB2.*blademag +...
302     ML2.*lowmag + MI2.*intmag + MU2.*upmag;
303 deflection1 = MR1.*rotormag + MB1.*blademag +...
304     ML1.*lowmag + MI1.*intmag + MU1.*upmag;
305
306 angle4 = atan((MR4.*rotormag + MB4.*blademag +...
307     ML4.*lowmag + MI4.*intmag + MU4.*upmag)./CoM1);
308 angle3 = atan((MR3.*rotormag + MB3.*blademag +...
309     ML3.*lowmag + MI3.*intmag + MU3.*upmag)./CoM3);
310 angle2 = atan((MR2.*rotormag + MB2.*blademag +...
311     ML2.*lowmag + MI2.*intmag + MU2.*upmag)./CoM2);
312 angle1 = atan((MR1.*rotormag + MB1.*blademag +...
313     ML1.*lowmag + MI1.*intmag + MU1.*upmag)./CoM1);
314
315 % ===== 9. Wind speeed probability ===== %
316 w_k = 2.47; w_a = 9.4; % Weibull distribution coeff.
317 windpdf = wpdf(windspeed,w_a,w_k)*10;
318
319 % ===== 10. Graphical results ===== %
320 figure()
321 plot(windspeed,windpdf.*100,'k'); grid on; grid minor;
322 xlim([0,36])
323 xlabel('Wind speed (m/s)');
324 ylabel('Occurance probability per unit time (%)');
325 title('Wind speed probability density function');
326
327 figure()
328 bodemag(F1x4,'k',F2x4,'g',F3x4,'b',F4x4,'r'); grid on; grid minor;
329 hold on;
330
331 legend
332 xline(f(1), '--'); xline(f(2), '--');
333
334
335 figure()
336 plot(X(1,:),y,'r',X(2,:),y,'b',-X(1,:),y,'r',-X(2,:),y,'b'); hold on;

```

```

337 scatter(0,CoM1,'r'); hold on; yline(CoM1,'--','Center of mass #1');
338 scatter(0,CoM2,'b'); hold on; yline(CoM2,'--','Center of mass #2');
339 scatter(0,CoM3,'g'); hold on; yline(CoM3,'--','Center of mass #3');
340 scatter(0,CoM4,'k'); hold on; yline(CoM4,'--','Center of mass #4');

341
342 grid on; axis equal; ylim([0 40]); xlim([-10 10]);
343 xlabel('Position (m)');
344 ylabel('Height (m)');
345 title('Cross section of the wind turbine tower');

346
347 figure()
348 subplot(211);
349 plot(windspeed,deflection4.*1000,'k'); hold on;
350 plot(windspeed,deflection3.*1000,'g');
351 plot(windspeed,deflection2.*1000,'b');
352 plot(windspeed,deflection1.*1000,'r');
353 grid on; grid minor; xlim([0,36])
354 legend
355 xlabel('Wind Speed (m/s)');
356 ylabel('Amplitute (mm)');
357 title('Translational Deflection');

358
359 xline(4,'--');xline(15,'--');xline(25,'--');
360
361 subplot(212);
362 plot(windspeed,angle4,'k'); hold on;
363 plot(windspeed,angle3,'g');
364 plot(windspeed,angle2,'b');
365 plot(windspeed,angle1,'r');
366 grid on; grid minor; xlim([0,36])
367 legend
368 xlabel('Wind Speed (m/s)');
369 ylabel('Amplitute (rad)');
370 title('Angular Deflection');

371
372 xline(4,'--');xline(15,'--');xline(25,'--');
373
374 % Matlab Functions
375
376 function Blade_Thrust_Force = btf(velocity)
377 p = [-1.55939516489868e-08,1.80111500882497e-06,-8.68167915894502e
378 -05,...,
379 0.00226048763000900,-0.0343971699472090,0.309594853153502,...,
380 -1.59488075063015,4.24399911328177,-3.53703531116710];
381
382 r_blade = 19.014;
383 Blade_Thrust_Force = (pi.*((r_blade).^2)./2 .*...

```

```

383     polyval(p,velocity) .* velocity .^ 2;
384 end
385
386 function k = springcons(D,t,g,h,E)
387 syms s
388 k = double(vpa((E*t*pi*(g^2 + 1)^(1/2))/(8*int((h - s)^2/((D - 2*g*s)
389 * ...
390 (4*g^2*s^2 + g^2*t^2 - 4*D*g*s + t^2 + D^2)), s, 0, h)),3));
391 end
392
393 function [ tfobj ] = sym2tf( symobj, Ts)
394 if isnumeric(symobj)
395     tfobj=symobj;
396     return;
397 end
398
399 [n,d]=numden(symobj);
400 num=sym2poly(n);
401 den=sym2poly(d);
402
403 if nargin==1
404     tfobj=tf(num,den);
405 else
406     tfobj=tf(num,den,Ts);
407 end
408 end

```

A.2.2 Optimization Study

Mass Optimization Main Code

```

1 % Linear equality constraint
2 % Tower height limit Aeq*x = beq
3 Aeq = [1 1 1 0 0 0 0 0 0];
4 beq = [35.37];
5
6 % Linear inequality constraint
7 % Aspect ratio Di+1<= Di
8 % Manufacturing constraint: ti-0.008Di <= 0
9 A = [0,0,0,1,0,0,-0.008,0,0,0;
10    0,0,0,0,0,0,0,1,-1;
11    0,0,0,0,0,0,0,1,-1,0];
12 b = [0,-0.001,-0.001];
13
14 % Lower and upper bounds
15 % Transportation constraint: 0<R1,R2,R3<2.5m
16 D_min = 0;

```

```

17 D_max = 5;
18 g_min=0.0001;
19 g_max=0.05;
20 h_min = 8;
21 h_max = 14;
22 t_min = [0.012,0.011,0.010];
23 t_max = 0.020;
24 lb = [h_min*ones(1,3),t_min.*ones(1,3),D_min,g_min*ones(1,3)];
25 ub = [h_max*ones(1,3),t_max*ones(1,3),D_max,g_max*ones(1,3)];
26
27 % Nonlinear constraints
28
29 % Tower property
30 G_r = 253.294e3; % Rotor equivalent axial load [N]
31 M_r = 289.610e3+248.030e3; % Rotor equivalent moment [Nm]
32 F_r = 139.810e3; % Rotor equivalent horizontal force [N]
33 pw1 = 4.7143e3; % Top section distributed wind load on
                     tower [N/m]
34 pw2 = 5.4280e3; % Mid section distributed wind load on
                     tower [N/m]
35 pw3 = 4.2288e3; % Bottom section distributed wind load on
                     tower [N/m]
36 RotationalSpeed= 25; % [rpm]
37 BladeNumber= 1;
38 % Material properties
39 E = 200e9; % [N/m^2] Young's modulus
40 v = 0.3; % [-] Poisson's ratio
41 f_y = 355e6; % [N/m^2] Yield stress:355MPa
42 beta = 0.02;
43 rho = 7800; % S355JR kg/m3
44
45 %% Main function for optimization
46 % Optimzation settings
47 options = optimoptions('fmincon');
48 options = optimoptions(options, 'Display', 'Iter');
49 options = optimoptions(options, 'MaxFunctionEvaluations',800000);
50 options = optimoptions(options, 'MaxIterations',50000);
51
52 % Initial guess to initialize the optimization algorithm
53 x0 = [12.03,12.04,11.3,0.018,0.018,0.015,2.2,0,0,0.04263];
54
55 MassInitial = massobjfunc([12.030,12.040,11.3,18e-3,18e-3,15e
-3,2.2,0,0,0.04263],7800)+...
    CalculateFlangeMass(rho,12.030,12.040,11.6,18e-3,18e-3,15e
-3,2.2,0,0,0.04263);
56
57 [x,fval] = fmincon(@(x)massobjfunc(x,rho),x0,A,b,Aeq,beq,lb,ub, ...

```

```

59             @(x)massoptnonlcon(x,G_r,M_r,F_r,pw1,pw2,pw3,rho,E,v
60             ,f_y,...;
61
62 MassOptimized=fval+CalculateFlangeMass(rho,x(1),x(2),x(3),x(4),x(5),x
63 (6),x(7),x(8),x(9),x(10));
64 [DampingRatio]= CalculateDampingRatio(x,rho,E);
65 [DampingRatioInitial]= CalculateDampingRatio([12.030,12.040,11.3,18e
66 -3,18e-3,15e-3,2.2,0,0,0.04263],7800,E);
67 [CostofTower]=CalculateCost(x,rho,MassOptimized);
68 [CostofTowerInitial]=CalculateCost([12.030,12.040,11.3,18e-3,18e-3,15e
69 -3,2.2,0,0,0.04263],7800,MassInitial);
70 [Stiffness ,~,~,~]=CalculateStiffnessAccurate(E,x(1),x(2),x(3),x(4),x(5)
71 ,x(6),x(7),x(8),x(9),x(10));
72 [StiffnessInitial ,~,~,~]=CalculateStiffnessAccurate(E
73 ,12.030,12.040,11.3,18e-3,18e-3,15e-3,2.2,0,0,0.04263);
74 %% Display
75 fprintf('-----Optimization results-----\n');
76 fprintf('Mass of current tower design: %d [kg].\n',MassInitial);
77 fprintf('Mass of optimized : %d [kg].\n',MassOptimized);
78 fprintf('Mass reduction : %f percent .\n',100*(MassInitial-
79 MassOptimized)/MassInitial);
80 fprintf('Cost reduction : %f percent .\n',100*(CostofTowerInitial-
81 CostofTower)/CostofTowerInitial);
82 fprintf('Stiffness: %f and increase: %f percent .\n',Stiffness,100*(
83 Stiffness-StiffnessInitial)/StiffnessInitial);

84 if DampingRatio<DampingRatioInitial
85     fprintf('Damping Ratio is less than the initial and reduction : %f
86     percent .\n',100*(DampingRatioInitial-DampingRatio)/
87     DampingRatioInitial)
88 else
89     fprintf('Damping Ratio is more than the initial and increase : %f
90     percent .\n',100*(DampingRatio-DampingRatioInitial)/
91     DampingRatioInitial)
92 end

```

Mass Objective Function

```

1 function f = massobjfunc(x,rho)
2
3 x1 = x(1); %H1
4 x2 = x(2); %H2
5 x3 = x(3); %H3
6 x4 = x(4); %t1
7 x5 = x(5); %t2

```

```

8 x6 = x(6); %t3
9 x7 = x(7); %D1
10 x8 = x(8); %g1
11 x9 = x(9); %g2
12 x10 = x(10); %g3
13
14 D2=x7-(2*x8*x1);
15 D3=D2-(2*x9*x2);
16
17 f = rho*pi*x6*sqrt(x10^2+1)*x3*(D3-x10*x3)...
18 + rho*pi*x5*sqrt(x9^2+1)*x2*(D2-x9*x2)
19 ...
+ rho*pi*x4*sqrt(x8^2+1)*x1*(x7-x8*x1);

```

Axial Load Calculation

```

1 function [effective_axial_load,D2,D3,D4,MassTower] = CalculateAxialLoad
2 (G_r,rho,L,H1,H2,H3,t1,t2,t3,D1,g1,g2,g3)
3 % Assumptions:
4 % Tower consists of 3 segments.
5 % Section1 (Base)
6 % Section2 (Middle)
7 % Section3 (Top)
8
9 % Parameters:
10 g = 9.81; %m/s^2;
11
12 D2=D1-(2*g1*H1);
13 D3=D2-(2*g2*H2);
14 D4=D3-(2*g3*H3);
15
16 % where y =
17 if L<=H3 && L>=0 % Refers to top section
18 effective_axial_load = G_r + rho*g*pi*t3*sqrt(g3^2+1)*(L)*(D3-g3*L-
19 g3*H3);
20
21 elseif L>H3 && L<=H2+H3% Refers to middle section
22 L=L-H3;
23 effective_axial_load = G_r + rho*g*pi*t3*sqrt(g3^2+1)*H3*(D3-g3*H3)
24 ...
25 + rho*g*pi*t2*sqrt(g2^2+1)*(L)*(D2-g2*L-
26 g2*H2);
27
28 elseif L>H2+H3 && L<=H1+H2+H3 % Refers to bottom section
29 L=L-H3-H2;
30 effective_axial_load = G_r + rho*g*pi*t3*sqrt(g3^2+1)*H3*(D3-g3*H3)
31 ...
32 + rho*g*pi*t2*sqrt(g2^2+1)*H2*(D2-g2*H2)

```

```

    ...
28             + rho*g*pi*t1*sqrt(g1^2+1)*(L)*(D1-g1*L-
g1*H1);
29
30 else
31     error('Invalid L definition. L should be between 0 and L_total')
32 end
33
34 MassTower= (effective_axial_load-G_r)/g;
35 end

```

Bending Moment Calculation

```

1 function [effective_axial_load,D2,D3,D4,MassTower] = CalculateAxialLoad
2     (G_r,rho,L,H1,H2,H3,t1,t2,t3,D1,g1,g2,g3)
3 % Assumptions:
4 % Tower consists of 3 segments.
5 % Section1 (Base)
6 % Section2 (Middle)
7 % Section3 (Top)
8
9 % Parameters:
10 g = 9.81; %m/s^2;
11
12 D2=D1-(2*g1*H1);
13 D3=D2-(2*g2*H2);
14 D4=D3-(2*g3*H3);
15
16 % where y =
17 if L<=H3 && L>=0 % Refers to top section
18     effective_axial_load = G_r + rho*g*pi*t3*sqrt(g3^2+1)*(L)*(D3-g3*L-
g3*H3);
19
20 elseif L>H3 && L<=H2+H3% Refers to middle section
21     L=L-H3;
22     effective_axial_load = G_r + rho*g*pi*t3*sqrt(g3^2+1)*H3*(D3-g3*H3)
23     ...
24         + rho*g*pi*t2*sqrt(g2^2+1)*(L)*(D2-g2*L-
g2*H2);
25
26 elseif L>H2+H3 && L<=H1+H2+H3 % Refers to bottom section
27     L=L-H3-H2;
28     effective_axial_load = G_r + rho*g*pi*t3*sqrt(g3^2+1)*H3*(D3-g3*H3)
29     ...
30         + rho*g*pi*t2*sqrt(g2^2+1)*H2*(D2-g2*H2)
31     ...
32         + rho*g*pi*t1*sqrt(g1^2+1)*(L)*(D1-g1*L-
g1*H1);

```

```

29
30 else
31     error('Invalid L definition. L should be between 0 and L_total')
32 end
33
34 MassTower= (effective_axial_load-G_r)/g;
35 end

```

Stiffness Calculation

```

1 function [S,S1,S2,S3]=CalculateStiffnessAccurate(E,H1,H2,H3,t1,t2,t3,D1
    ,g1,g2,g3)
2 D2=D1-(2*g1*H1);
3 D3=D2-(2*g2*H2);
4 InitialStiffness=7.4030e+06;
5 % Sectional stiffness
6
7 S1 = springcons(D1,t1,g1,H1,E);
8 S2 = springcons(D2,t2,g2,H2,E);
9 S3 = springcons(D3,t3,g3,H3,E);
10
11 % Total stiffness
12 S = ((1/S1)+(1/S2)+(1/S3))^-1;
13
14 end

```

Damping Ratio Calculation

```

1 function [S,S1,S2,S3]=CalculateStiffnessAccurate(E,H1,H2,H3,t1,t2,t3,D1
    ,g1,g2,g3)
2 D2=D1-(2*g1*H1);
3 D3=D2-(2*g2*H2);
4 InitialStiffness=7.4030e+06;
5 % Sectional stiffness
6
7 S1 = springcons(D1,t1,g1,H1,E);
8 S2 = springcons(D2,t2,g2,H2,E);
9 S3 = springcons(D3,t3,g3,H3,E);
10
11 % Total stiffness
12 S = ((1/S1)+(1/S2)+(1/S3))^-1;
13
14 end

```